The Canadian Mineralogist
Vol. 43, pp. 105-128 (2005)

STAUROLITE AND OTHER ALUMINOUS PHASES IN ALPINE ECLOGITE FROM THE CENTRAL SWISS ALPS: ANALYSIS OF DOMAIN EVOLUTION

FRAUKJE M. BROUWER§ AND MARTIN ENGI§

Institute of Geological Sciences, University of Bern, Baltzerstrasse 1, CH–3012 Bern, Switzerland

ABSTRACT

Kyanite eclogite in the Central Swiss Alps, partially hydrated during decompression, shows conspicuous domains containing unusual phases, such as staurolite, corundum, and hercynite-dominant spinel. Detailed analysis of these domains indicates that they formed by prograde growth of porphyroblasts of lawsonite, kyanite, and garnet, prior to the complete conversion of igneous plagioclase to omphacite. In the evolution following the culmination in pressure, the chemically differentiated domains remained largely distinct from the matrix. Quantitative thermodynamic models set up for each domain allow us to analyze each domain type, in order to test (a) to what extent they behaved as closed systems, (b) whether local equilibrium was maintained during decompression, and (c) what reaction mechanisms and volumes were involved in the observed transformations. Results indicate that metasomatic effects were quite limited; local equilibration was possible to mid-crustal levels at temperatures near 700°C; reaction paths followed involved minimal transport of Al. Both prograde and retrograde parts of the P–T path could be deduced for eclogite samples from the Southern Steep Belt of the Central Swiss Alps. A late-orogenic, prograde thermal overprint (heating spike) is confirmed.

Keywords: reaction volume, kyanite eclogite, decompression, thermodynamic modeling, local equilibrium, DOMINO program, Swiss Alps.

SOMMAIRE

Les éclogites à kyanite des Alpes suisses centrales, partiellement hydratées au cours de la décompression, font preuve de domaines bien visibles contenant des minéraux inhabituels, par exemple staurolite, corindon, et un spinelle à dominance de hercynite. Une analyse détaillée de ces domaines montre qu'ils se sont formés par croissance prograde de porphyroblastes de lawsonite, kyanite, et grenat, avant la conversion complète du plagioclase igné en omphacite. Au cours de l'évolution suivant le paroxysme en termes de pression, les domaines chimiquement différenciés sont restés distincts de la matrice. Des modèles thermodynamiques quantitatifs établis pour chaque domaine nous permettent d'analyser chaque type de domaine afin de savoir (a) à quel point ils se sont comportés en systèmes fermés, (b) si l'équilibre local a été maintenu au cours de la décompression, et (c) quels mécanismes et volumes de réaction ont été impliqués dans les transformations observées. Les résultats indiquent que les effets métasomatiques ont été assez limités; l'équilibrage local pendant la décompression a été possible à un niveau équivalent au milieu de la croûte, à des températures d'environ 700°C, et les séquences de réaction ont été régies par la distance minimale de transfert de l'aluminium. On peut en déduire les tracés prograde et rétrograde de l'évolution P–T des échantillons d'éclogite provenant du "Southern Steep Belt" des Alpes centrales suisses. L'importance d'un événement thermique prograde tardi-orogénique (pointe thermique surimposée) est confirmée.

(Traduit par la Rédaction)

Mots-clés: volume de réaction, éclogite à kyanite, décompression, modèle thermodynamique, équilibre local, logiciel DOMINO, Alpes suisses.

§ *E-mail address*: brouwer@geo.unibe.ch, engi@geo.unibe.ch

Introduction

Eclogites from various places in the world have been reported to contain symplectites of plagioclase and Al-rich minerals such as corundum, Fe–Mg-bearing spinel and sapphirine surrounding relics of kyanite or zoisite (*e.g.,* Dal Vesco 1953, Lappin 1960, Liati & Seidel 1994). Staurolite has been reported as a product of secondary replacement in eclogites from eastern China (Enami & Zang 1988) and Greenland (Elvevold & Gilotti 2000). As several investigators have noted, such aluminous phases would not be expected in rocks of basaltic bulk composition if these rocks behaved as a single equilibration volume. The development of compositionally differentiated domains during metamorphism may indicate spatial limits to thermodynamic equilibrium and implies at least grain-scale mass transfer. Disequilibrium considerations have made some authors reluctant to apply equilibrium models in order to draw conclusions on the conditions of formation of symplectites (*e.g.,* Elvevold & Gilotti 2000, Sabau *et al.* 2002). Yet, on the basis of an assumption of local chemical equilibrium, an elegant kinetic model was recently developed for the decompression of kyanite eclogites (Nakamura 2002). It showed how chemical potential gradients of Na_2O and CaO due to garnet and clinopyroxene breakdown cause the formation of a plagioclase mantle between kyanite and quartz. Local SiO_2 undersaturation within this mantle allows kyanite to survive decompression. Even in the presence of an aqueous fluid, such undersaturation prevents reactions with garnet, clinopyroxene and quartz, which would otherwise produce amphibole and plagioclase. In this SiO_2-deficient area, corundum and Fe–Mg-bearing spinel may develop, although free quartz is ubiquitous outside the plagioclase mantle.

The current study of symplectites from the Central Alps is also based on an assumption of local equilibrium. Using careful estimates of the "bulk" chemical composition of the various symplectite domains observed, we investigate to what extent equilibrium thermodynamic models can predict assemblages of minerals observed in kyanite eclogite symplectites, notably those leading to the appearance of corundum, hercynite-dominant spinel, and staurolite. One goal of the study is to analyze whether and under which conditions it is possible to model particular mineralogical and textural domains using a strictly equilibrium thermodynamic approach. We realize that although the geometry of corona structures and symplectites provides petrographic evidence of limited chemical interaction with their chemically different surroundings, it is not trivial to use these observations to infer reaction volumes. Retrograded eclogites may have complex pressure – temperature – deformation (P–T–D) paths, and the chemical contents, mobility and episodic interaction with fluids are certain to have varied along the prograde and retrograde metamorphic paths followed by these rocks. However, such rocks may provide information on petrogenetic conditions and processes at several stages of their evolution, or on how the domains formed in the first place, and to what extent they may be regarded as closed systems subsequently. We aim to show that under certain conditions, useful models can be developed that allow an assessment of the actual volumes of equilibration, an interpretation of the texture, inferences on likely precursor phases, and an estimate of the P–T conditions at which hercynite-dominant spinel, corundum and staurolite may be stabilized in eclogites.

Methods

This study relies on a comparison of stable phase-assemblages computed for a specified bulk-composition with those documented in kyanite eclogite samples. With the programs Domino and Theriak (De Capitani 1994), we calculate the complete, stable assemblage of minerals for each point in a P–T grid for a given bulk-composition. These programs can be used to constrain the conditions at which a given assemblage of minerals equilibrated, as well as possible precursor assemblages. Inversely, where the models fail to reproduce the observed assemblage, inferences can be made regarding the accuracy of the estimated bulk-composition, gains or losses of components from the domain, and the possibility of disequilibrium among the phases present within the domain.

Accurate modeling of the evolution of assemblages of metamorphic minerals is possible only where the chemical composition within a reaction volume (or equilibration volume) is known. Conventional bulk-compositions are not appropriate in this study because mm-size domains, containing quartz-undersaturated metamorphic assemblages, occur in a matrix with free quartz. Effective reaction-volumes thus probably were of the same magnitude as the domains observed. Where possible, we selected domains in a thin section such that they correspond roughly to a central section. We then assumed that the total surface-area of each mineral reflects its modal abundance and converted these modes to an effective bulk-composition using averaged results of electron-microprobe analyses. This procedure is a rough approximation at best, for at least two reasons: (a) for domains of ovoid or spheroid shape, the contribution of the rim composition would be underestimated; (b) for any shape, a section far from the center of a domain would underestimate the contribution of the core. In the absence of precise data for (b) from either tomography or systematic sectioning, and in view of the prismatic or lozenge-shaped domains analyzed here, it seems difficult to improve upon the simple assumption made.

We reconstruct the local bulk-composition for each type of domain by analysis of back-scattered electron images and, where necessary, use of X-ray maps (both on Camscan CS4 SEM, University of Bern). Electron-

microprobe analyses were performed using a Cameca SX–50 (15 kV and 20 nA) at the University of Bern. Synthetic and natural mineral standards were used, and PAP corrections applied.

In modeling the domain, modal abundances and normalized compositions of minerals are selected to calculate a preliminary bulk-composition as input for DOMINO. This approach implies a certain amount of judgment regarding the delimitation of any domain against its neighbors, as well as the selection of specific analytical data (or means thereof) for minerals contained within the domain. Out of the four examples presented below, preliminary calculations using THERIAK for two cases (A, B) showed that the initial choices of domain boundaries led to predicted assemblages of minerals that reproduced the observed assemblages and compositions of minerals. In the two other cases (domains C and D), it was not evident how much quartz was effectively part of the domains, because they are surrounded by free quartz. Our initially estimated bulk-compositions included 6 and 5 vol.% of quartz, respectively, but preliminary calculations showed that this additional SiO_2 had to be removed for the stable assemblages of minerals predicted to approach the observations closely.

An essential condition for the success of our approach is the availability of adequate thermodynamic models, including solution models, for *all* phases with a potential stability-field in the P–T region of interest. The thermodynamic database used in this study is an extended version of the database of Berman (1988), with internally consistent additions by Meyre *et al.* (1997) for omphacite (diopside, jadeite and hedenbergite endmembers), Meyre *et al.* (1999) for annite, glaucophane, ferroceladonite and celadonite, and Nagel (2002) for staurolite and Fe-dominant chlorite. Also added were an ideal speciation model for hercynite-dominant spinel (based on Engi 1983), a regular asymmetric model for cummingtonite–grunerite amphiboles (based on data from Ghiorso *et al.* 1995), and a new site-occupancy model for Fe–Mg-bearing hornblende, based on Mäder & Berman (1992) for the pseudobinary join actinolite – pargasite. The latter two models are but first-order approximations to describe the amphiboles occurring as minor phases in some of the coronas. A complete copy of the thermodynamic database used is available from the Depository of Unpublished Data, CISTI, National Research Council, Ottawa, Ontario K1A 0S2, Canada, or from the authors on request.

Geological Context and Sample Description

The Southern Steep Belt (SSB) in the Central Alps of southern Switzerland (Fig. 1a) is largely made up of a composite of granitic gneisses, metaclastic schists, marbles and calc-silicate rocks that incorporates centimeter- to kilometer-scale lenses of mafic and ultramafic material. Some rock types in this high-strain zone preserve relics of high-pressure metamorphism, and all show evidence of subsequent Barrovian high-temperature metamorphism at intermediate pressure, which caused extensive migmatization in the felsic and intermediate lithologies enveloping the mafic lenses.

The SSB is considered to represent an exhumed portion of a tectonic accretion channel (TAC, Engi *et al.* 2001) related to the Tertiary collision of Eurasia with the Apulian promontory of Africa (Schmid *et al.* 1989, 1996). This TAC is a mélange zone 5–8 km in thickness, which formed at the contact of the subducting slab and the overriding plate. The TAC accommodates tectonic fragments considered to be derived from both plates during the subduction, accretion, and exhumation. We note that in the context of such a TAC, it is expected that lenses may record different P–T trajectories within the same thermal-tectonic regime, and that the exhumed channel behaved as a tectonic mélange, rather than a coherent nappe, at least during initial parts of the history. In the Adula nappe, which represents a part of this same mélange unit (partly outside the SSB), the partial hydration and amphibolite-facies overprint of eclogite lenses upon decompression have long been established (Heinrich 1986).

The samples selected for the current study were collected from two lenses of kyanite eclogite at Gorduno (indicated in Fig. 1b), near Bellinzona in the Central Swiss Alps (Grubenmann 1908, Möckel 1969). Eclogites from the Gorduno area have a tholeiitic bulk-composition (Bocchio *et al.* 1985). The lenses are mostly made up of biotite and garnet amphibolites, but occasional relics of kyanite and very rarely omphacite are preserved. Conditions of high-pressure metamorphism were in the range 750 ± 50°C at 23 ± 3 kbar (Tóth *et al.* 2000). Relics of the high-pressure assemblage are usually surrounded by symplectites of hornblende and plagioclase around garnet, and of amphibole ± clinopyroxene + plagioclase replacing omphacite. The rare occurrence of spinel and corundum in symplectites around kyanite was previously noted (Dal Vesco 1953, Möckel 1969, Bocchio *et al.* 1985), and recently a first attempt at retrieving information about the conditions of their formation yielded an estimate of 750 ± 40°C at 8 ± 1 kbar (Tóth *et al.* 2000). Figure 2 is an equilibrium phase-diagram for an average bulk-composition of Gorduno eclogite, which we consider representative of the samples presented in this study (Table 2, adapted from Bocchio *et al.* 1985), with hydrous fluid added. It indicates the typical parageneses of minerals one would expect for a fully equilibrated eclogite, hydrated during decompression. At the conditions of the Barrovian overprint, the predicted assemblage is dominated by hornblende and intermediate plagioclase, with additional cummingtonite (10 vol.%), omphacite (8%), ilmenite (1.7%) and H_2O. It is notable that none of the aluminous phases mentioned above are predicted to occur for this bulk composition.

In the present study, we focus on four types of coronas from three samples of garnet amphibolites highly

affected by symplectite formation. Garnet in these rocks is invariably surrounded by a rim of amphibole and plagioclase, locally with secondary (low-Na) clinopyroxene. Very few relics of primary omphacite remain; most of it was replaced by very fine symplectitic intergrowths of secondary clinopyroxene, amphibole and plagioclase. The samples contain symplectites dominated by plagioclase and aluminous phases like kyanite, hercynite-dominant spinel, corundum and staurolite, in which amphibole is very rare. Figure 3 depicts a typical sample in hand specimen, in which the size and distribution of different corona domains are quite visible. Four examples of such coronas are investigated in detail below: domain A: high-An plagioclase with hercynite and corundum, domain B: kyanite and staurolite, domain C: garnet and corundum, and domain D:

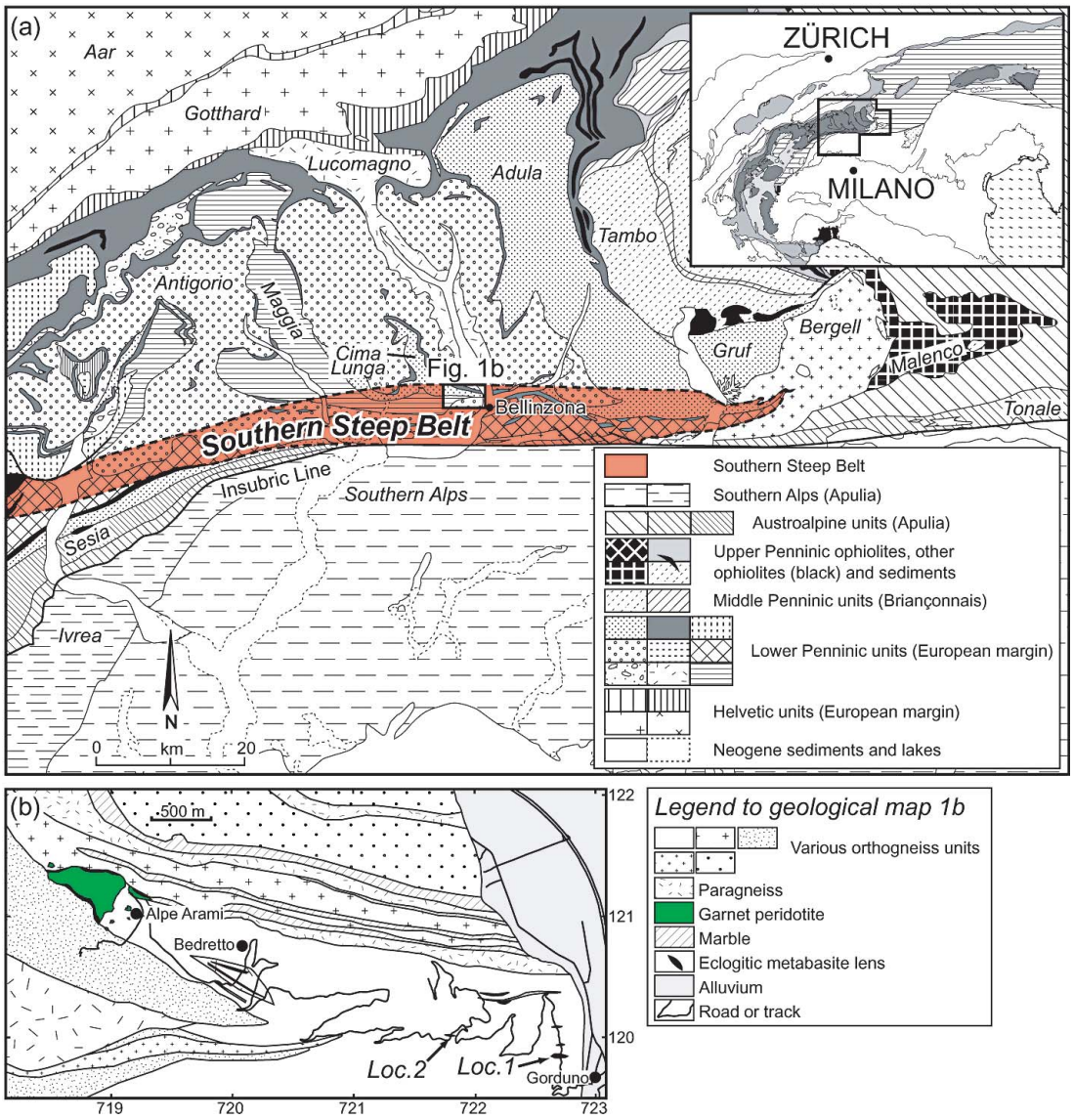

FIG. 1. (a) Tectonic map of the Central Swiss Alps. The Southern Steep Belt is the region where exhumed units are steeply oriented along the Insubric Line, marked in light red. Location of the map shown in (b) is indicated. After Pfiffner & Trommsdorff (1998). (b) Geological map indicating the locations of the kyanite eclogite boudins from which the samples studied were collected. After Bächlin *et al.* (1974).

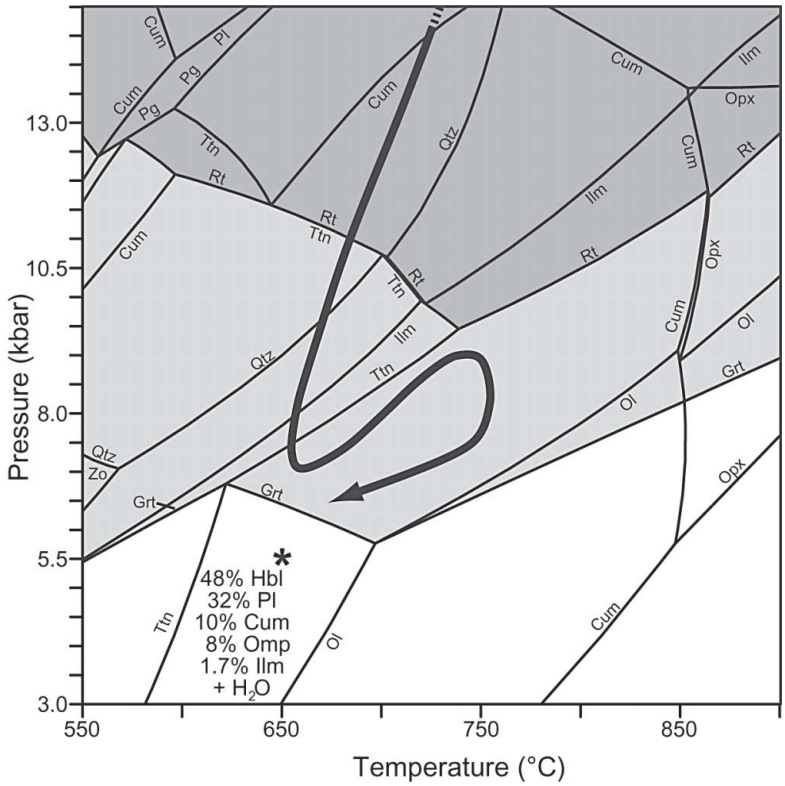

FIG. 2. TCNFMASH equilibrium phase-diagram computed with DOMINO for average Gorduno eclogite (after Bocchio *et al*. 1985; Table 2), with hydrous fluid added. The P–T path is for retrograded eclogites from Gorduno (Tóth *et al*. 2000). The predicted fully equilibrated hydrous amphibolite-facies assemblage is listed for 650°C, 5.5 kbar (star), the conditions for the regional Barrovian overprint. The compositions of the phases at that stage, computed using THERIAK, are given in Table 3. Reaction labels indicate the appearence of new phases; shaded fields denote the stability of garnet (light grey) and garnet + rutile (dark grey). Upon decompression, at around 10 kbar, rutile is predicted to disappear from the eclogite assemblage, followed by garnet at around 6 kbar. Abbreviations mostly follow Kretz (1983); all are listed in Appendix 1.

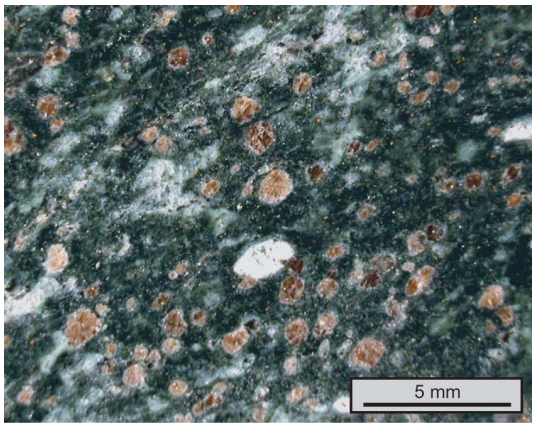

FIG. 3. Polished slab of sample Ma9338 showing garnet relics (pink) in a matrix dominated by hornblende (black) and plagioclase (white). Garnet is rimmed by hornblende + plagioclase symplectite. The bright corona near the center of the image is domain A, consisting of plagioclase with tiny inclusions of corundum and spinel. Domain A is discussed in detail below.

kyanite and hercynite. Samples AA97–16.1 (with domain B) and AA97–14.2 (domains C and D) were collected from the same eclogite boudin (Loc. 2 in Fig. 1b, Swiss coordinates 721.8/120.0/690m). Although they have experienced the same pressure–temperature evolution, they may well have recorded different stages along this trajectory. Since sample Ma9338 (with domain A) was collected from a different boudin (Loc. 1 in Fig. 1b, 722.7/119.9/390m) within the mélange sequence, it may have gone through a significantly different P–T history. A precursor study by Tóth *et al.* (2000) concentrated on garnet domains at this same locality; therefore, this type of domain is not investigated further here.

TABLE 1. MODAL ANALYSIS, COMPOSITION OF MINERALS AND ESTIMATED BULK-COMPOSITION DOCUMENTED FOR THE DOMAINS

Domain	A	B	C	D
Sample	Pl Ma9338a	Ky+St AA97-16.1	Grt+Crn AA97-14.2	Ky+Spl AA97-14.2
Modes of minerals in each domain				
Pl	0.94	0.74	0.65	0.66
Bt			0.15	0.08
Chl			0.01	
Crn	0.002		0.04	
Cum		0.04		
Grt			0.07	
Hbl	0.006	0.001	0.02	0.01
Ilm	0.001	0.0004	0.0004	0.003
K-phase	0.03	0.001		
Ky		0.10		0.16
Ms	0.003			
Opx			0.01	0.0004
Qtz		0.06	0.06	0.05
Rt			0.0002	
Spl	0.01			0.05
St		0.06		
Total	1.00	1.00	1.00	1.00
Solid solutions				
Pl	An_{99}	An_{33}	An_{31}	An_{32}
Bt			X_{Mg} 0.59	X_{Mg} 0.61
Cum		X_{Mg} 0.64		
Grt			$Grs_{23}Alm_{55}Prp_{22}$	
Hbl	X_{Mg} 0.68	X_{Mg} 0.61	X_{Mg} 0.67	X_{Mg} 0.64
Opx			X_{Mg} 0.60	X_{Mg} 0.60
Spl	Hc_{71}			Hc_{75}
St		X_{Mg} 0.31		
Bulk compositions*				
	A'	B'	C'	D'
SiO_2 wt%	44.58	57.92	54.53	53.09
TiO_2	0.04	0.05	0.56	0.40
Al_2O_3	35.66	27.93	24.76	31.19
Cr_2O_3	0.01	0.01	0.01	0.01
Fe_2O_3	0.12	0.22	0.24	0.18
FeO	0.42	1.59	4.58	3.00
MnO	0.01	0.04	0.10	0.04
MgO	0.18	1.12	2.86	1.39
CaO	17.56	5.11	4.94	4.40
Na_2O	1.13	5.71	5.10	5.06
K_2O	0.25	0.07	1.66	0.91
H_2O	0.03	0.22	0.66	0.33
Total	100.00	100.00	100.00	100.00

* based on area and chosen compositions of minerals.

Domain A: High-An Plagioclase with Hercynite and Corundum

In this and the following sections, we summarize results of our petrographic and microchemical study of four types of domains observed in the three samples of kyanite eclogite described above. These data are presented in comparison to the thermodynamic models and inferences therefrom regarding possible precursor phases in each domain.

Appendix 2 lists averaged results of electron-microprobe analyses of the phases found in each domain (A – D). Table 1 contains modal abundances of all phases in these and, in the case of solid solutions, their mineral compositions; in addition, the preliminary estimates (A' – D') of local bulk-compositions computed from the above data are given. Table 2 lists the simplified bulk compositions used as input for Theriak and Domino, as well as the slightly adjusted input compositions (A", C", and D") used in further modeling. Table 3 contains the modal abundances and compositions of minerals that define stable assemblages calculated for specific points, indicated with stars in the corresponding P–T diagrams.

TABLE 2. SIMPLIFIED BULK-COMPOSITIONS AND Domino INPUT FOR EACH OF THE DOMAINS

Domain	A'	A"	B'	C'	C"	D'	D"	Bocchio
Sample	Pl Ma 9338a	wet	Ky+St AA97- 16.1	Grt+Crn AA97- 14.2	no Qtz	Ky+Spl AA97- 14.2	no Qtz	average Gorduno eclogite*
Simplified bulk-compositions for each domain								
SiO_2 wt%	44.72	45.06	58.24	54.96	52.19	53.51	51.26	48.79
TiO_2				0.56	0.59	0.41	0.43	1.38
Al_2O_3	35.80	36.07	27.93	24.96	26.50	31.10	32.61	15.20
FeO	0.57	0.00	1.82	4.84	5.13	3.14	3.29	10.31
MgO	0.18	0.00	1.13	2.89	3.06	1.40	1.47	9.66
CaO	17.60	17.73	5.14	4.98	5.29	4.41	4.63	11.50
Na_2O	1.13	1.14	5.74	5.14	5.45	5.08	5.32	3.16
K_2O				1.67	1.77	0.94	0.99	
Sum	100.00	100.00	100.00	100.00	100.00	100.00	100.00	100.00
Input for Domino (molar units)								
	A'	A"	B'	C'	C"	D'	D"	Bocchio
Si	742.3	742.3	965.5	907.6	861.4	887.1	849.7	807.6
Ti				7.0	7.4	5.1	5.4	17.2
Al	700.3	700.3	545.7	485.7	515.5	607.7	637.1	296.6
Fe^{2+}	7.9		25.2	66.8	70.8	43.5	45.5	142.6
Mg	4.6		27.9	71.1	75.4	34.7	36.3	238.3
Ca	313.0	313.0	91.3	88.1	93.5	78.4	82.2	203.9
Na	36.3	36.3	184.5	164.4	174.5	163.2	171.1	101.4
K				35.2	37.3	19.9	20.8	
H	3.1	1500.0	24.2	72.9	77.3	36.4	38.1	13.5
O	2880.25	3616.2	2998.3	2920.0	2895.1	2962.3	2944.9	2736.8

* The average bulk-composition of five samples of eclogite from the Gorduno suite is listed for comparison (Bocchio *et al.* 1985).

Characterization of domain A

The overall corona in sample Ma9338a is oval in shape, slightly larger than 1 × 2 mm, and is made up of mostly plagioclase. It is surrounded by a mixture of calcic amphibole with fine plagioclase (Figs. 4a, b). The lower edge of the domain abuts against two smaller garnet domains, rimmed by plagioclase and amphibole, which impinge on the outer rim of plagioclase in that section. The domain has an outer rim of plagioclase with An_{30-50} (Fig. 4c), which includes one large grain of apatite (~200 μm) and rutile (60 μm) each. The inner portion of the corona is texturally different, with much more conspicuous grain-boundaries and ubiquitous fine inclusions. The shape of this zone is reminiscent of lawsonite or zoisite (Fig. 4b), and it is made up of mostly plagioclase, with a composition of An_{78-98} (mean An_{90}). The inner zone contains tiny inclusions of ilmenite, as well as a phase that is so fine-grained we have been unable to analyze it well. "Mixed-target" microprobe data com-

TABLE 3. STABLE ASSEMBLAGES OF MINERALS AND THEIR COMPOSITIONS, AS PREDICTED BY THERIAK FOR GIVEN BULK COMPOSITIONS AND P–T CONDITIONS, ALPINE ECLOGITES FROM THE CENTRAL SWISS ALPS

Bulk, P, T	Phase	Vol.%	Composition	Bulk, P, T	Phase	Vol.%	Composition
Bocchio wet	Hbl	48.0	X_{Mg} 0.80	C"	Pl	53.3	$Ab_{82}An_{15}Or_3$
	Pl	32.4	$An_{49}Ab_{51}$		Grt	16.6	$Alm_{47}Grs_{27}Prp_{26}$
650°C	Cum	10.1	X_{Mg} 0.43	700 °C	Phg	13.8	$Ms_{85}Cel_{12}FeCel_3$
5.5 kbar	Omp	1.0	$Jd_2Di_{45}Hd_{53}$	16.0 kbar	Omp	7.5	$Jd_{59}Di_{32}Hd_9$
Fig. 2, *	Ilm	1.7			Hbl	4.9	X_{Mg} 0.98
	Steam	77.2			Crn	3.5	
					Rt	0.4	
A`	Pl	97.4	$An_{90}Ab_{10}$				
	Grt	1.1	$Alm_{59}Grs_{13}Prp_{28}$	C"	Omp	52.9	$Jd_{69}Di_{20}Hd_{11}$
675°C	Crn	1.0			Phg	17.5	$Ms_{71}Cel_{23}FeCel_6$
6.5 kbar	Spl	0.3	Hc_{66}	700°C	Ky	15.0	
Fig. 6, *	Hbl	0.2	X_{Mg} 0.91	20.0 kbar	Grt	9.2	$Alm_{59}Grs_{20}Prp_{21}$
	Steam	1.3			Qtz	4.3	
					Pg	0.6	
A'	Pl	97.7	$An_{90}Ab_{10}$		Rt	0.5	
	Crn	0.9					
675°C	Spl	0.6	Hc_{70}	D"	Pl	73.9	$Ab_{66}An_{32}Or_2$
5.5 kbar	Grt	0.5	$Alm_{64}Grs_9Prp_{27}$		Sil	15.4	
Fig. 6, +	Cum	0.3	X_{Mg} 0.58	720°C	Bt	6.6	X_{Mg} 0.62
	Steam	1.1		5.0 kbar	Spl	3.5	Hc_{74}
				Fig. 12a	Ilm	0.5	
A"	Lws	88.6			Crn	0.03	
	Pg	6.9			Steam	3.7	
400°C	Omp	2.9	Jd_{100}				
14.0 kbar	Qtz	1.5		D"	Pl	75.5	$Ab_{66}An_{31}Or_3$
Fig. 7b, *	Steam	105.0			Ky	7.3	
				730°C	Bt	5.5	X_{Mg} 0.63
A"	Zo	68.8		9.0 kbar	St	4.2	X_{Mg} 0.31
	Pg	15.3		Fig. 12a	Grt	3.8	$Alm_{69}Grs_8Prp_{23}$
550°C	Ky	8.6			Crn	3.4	
14.0 kbar	Qtz	7.3			Rt	0.3	
Fig. 7b, +	Steam	635.5					
				D"	Pl	75.9	$Ab_{66}An_{30}Or_4$
A"	Pl	98.1			Ky	8.4	
675°C	Sil	1.0		760 °C	Grt	5.9	$Alm_{65}Grs_7Prp_{28}$
6.5 kbar	Crn	0.9		9.5 kbar	Bt	4.9	X_{Mg} 0.64
Fig. 7b, o	Steam	750.0		Fig. 12a	Crn	4.6	
					Rt	0.3	
B'	Pl	77.8	$An_{33}Ab_{67}$		Steam	8.0	
	Ky	7.6					
600°C	Qtz	6.2		D"	Omp	51.7	$Jd_{70}Di_{14}Hd_{16}$
7.0 kbar	Cum	4.4	X_{Mg} 0.59		Ky	30.5	
Fig. 9, *	St	4.0	X_{Mg} 0.31	700°C	Phg	9.0	$Ms_{83}Cel_7FeCel_{10}$
				20 kbar	Qtz	5.8	
B'	Qtz	20.4			Grt	1.5	$Alm_{43}Grs_{50}Prp_7$
	Omp	48.0	$Jd_{77}Di_{12}Hd_{11}$		Kfs	0.7	$Ab_{10}Or_{90}$
700°C	Ky	21.8			Ttn	0.7	
20.0 kbar	Zo	8.7			Rt	0.1	
	Pg	1.1					
C"	Pl	77.2	$Ab_{64}An_{34}Or_2$				
	Bt	14.1	X_{Mg} 0.65				
725°C	Grt	4.7	$Alm_{67}Grs_5Prp_{28}$				
6.5 kbar	Crn	3.4					
Fig. 11, *	Ilm	0.7					
	Steam	6.1					

The amount of free H_2O present as steam is given in moles. The symbols *, + and o after the figure numbers correspond to symbols in the P-T diagrams.

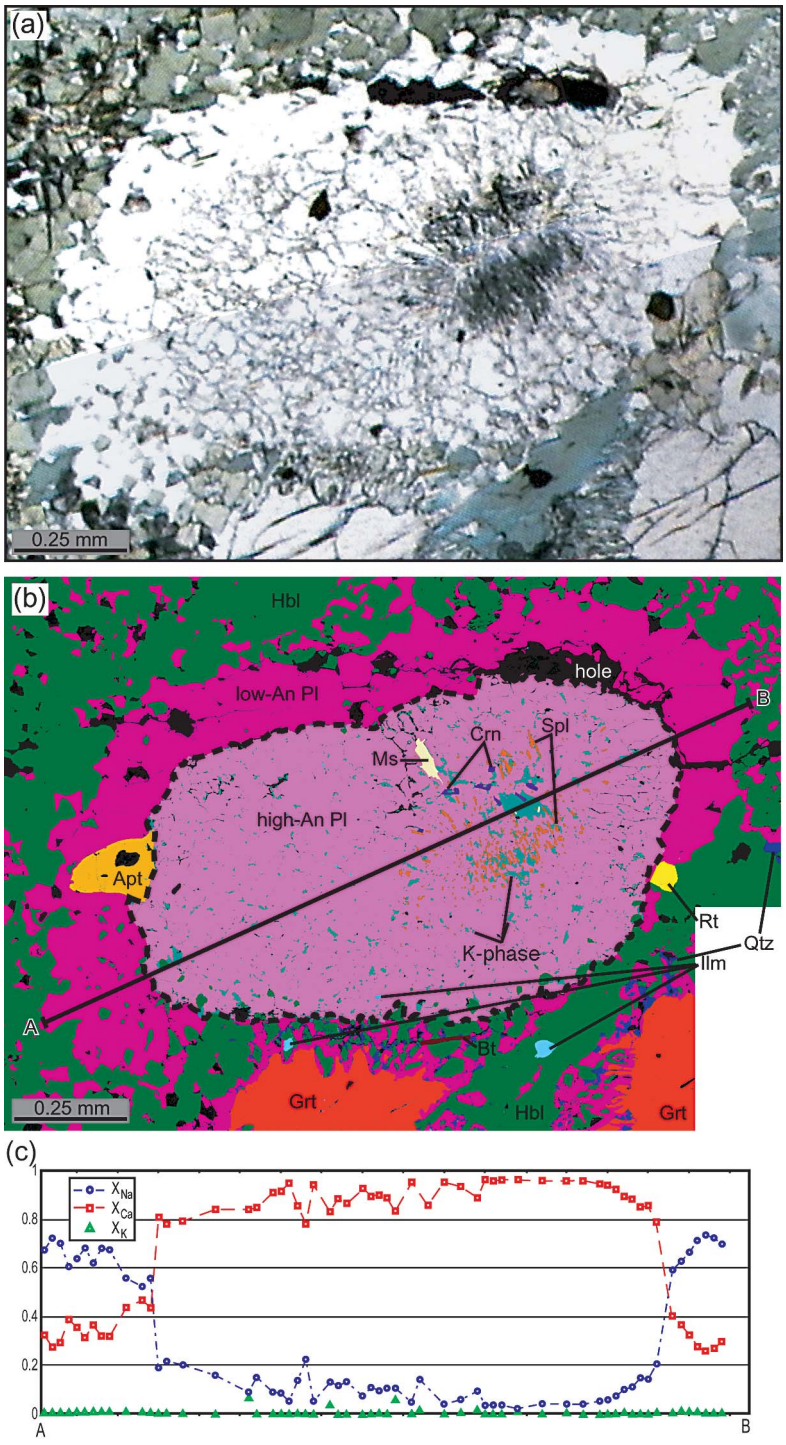

FIG. 4. Domain A. (a) Thin section photograph in plane-polarized light. (b) Back-scattered SEM image with indexed colors. (c) Variation of plagioclase components in electron-microprobe analyses along the transect indicated in Figure 4b.

monly yield low totals. Only Si, Al, Ca, Na and K (up to 7.7 wt% K_2O) were detected, and the SiO_2 content is consistently higher than for plagioclase (but always <58 wt%). Based on these findings, K-feldspar would seem a likely candidate. As the compositions plot in the "forbidden zone" of the feldspar diagram, plagioclase and K-feldspar would have coexisted at some stage. However, micro-Raman spectra of the potassic phase correspond neither to the spectrum of K-feldspar nor that of muscovite, phlogopite or leucite. Because it has not been possible to identify the potassic phase, and the total amount of K in the domain is but 0.25 wt% K_2O (Table 1), we chose to omit that component from further analysis. The inner zone contains a few grains of corundum, as well as strings of hercynite ($Hc_{71}Spl_{29}$). In the core of the inner zone, a few grains of pure muscovite occur, which are roughly lined up along a crack, whereas the outside includes some grains of magnesiohornblende.

The inner zone of high-An plagioclase (light pink in Fig. 4b) with its inclusions is called domain A and regarded as a remnant of some porphyroblast, which was not visibly affected by diffusional equilibration with the matrix. (In contrast, the outer rim is attributed to such interaction.) It is noteworthy that the range of compositions in the inner domain suggests plagioclase straddling the Huttenlocher gap (Carpenter 1985), whereas the outer zone may reflect the Bøggild gap for temperatures of ~600°C.

Neither apatite nor rutile is considered part of domain A. Ti and K (as discussed above) are present in very limited amounts; hence they were left out of the simplified bulk-composition of the domain (A' in Table 2). Figure 5 shows an ACF plot of the bulk composition of the eclogite sample and the plagioclase-rich domain (as well as the domains presented below) and thus depicts some of the effect of metamorphic differentiation in the sample.

Model for the retrograde assemblage

The equilibrium phase-diagram computed with the program DOMINO for the estimated bulk-composition A' is depicted in Figure 6. Owing to the absence of quartz, the stability field of corundum is large and overlaps to a major extent that of the Fe–Mg-bearing spinel. Isopleths for hercynite in the Fe–Mg-bearing spinel indicate formation temperatures of 600–700°C at pressures below about 8 kbar. If the magnesiohornblende occurring in the rim of the domain is included in equilibrium considerations, the P–T conditions are constrained to 6.5 ± 1 kbar and 675 ± 25°C (shaded field in Fig. 6). Because of uncertainties in the solution model for amphibole, and owing to the low modal abundance of magnesiohornblende, its exact composition cannot be used to further constrain the equilibrium conditions. Within the indicated field of stability, garnet is also predicted to occur, albeit again at very low modal abundance (~1 vol.%; Table 3). Garnet is missing in the present section through the domain, but its presence in other sections through this domain cannot be excluded.

Because K was left out of the simplified bulk-composition, muscovite and K-feldspar do not appear in the computed equilibrium phase-diagram. Muscovite flakes are associated with a crack, and we believe that muscovite formed in response to an influx of aqueous fluid.

Precursor

As noted above, the shape of the present domain is reminiscent of lawsonite or zoisite, and the predominance of bytownite indicates that these minerals are indeed likely precursors for the domain. These possibilities can be assessed in a binary phase-diagram, computed for a simplified bulk-composition A" (Table 2) with variable amounts of H_2O *versus* temperature at a pressure within the stability fields of lawsonite and zoisite, arbitrarily set at 14 kbar. In comparison with

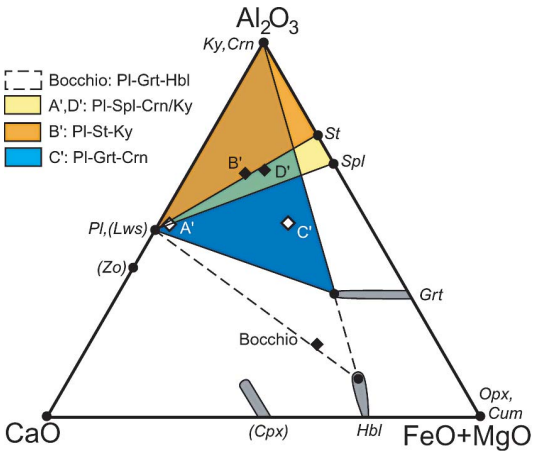

FIG. 5. ACF plot with the bulk compositions calculated for each of the domains, as well as the average bulk-composition of the Gorduno eclogite from Bocchio *et al.* (1985). Notably, the calculated compositions of the domains plot in different places, all far from the eclogite whole-rock composition. Projection from SiO_2 and H_2O. Closed diamonds represent quartz-saturated bulk compositions, open diamonds are quartz-undersaturated. Colored fields refer to assemblages formed during decompression reactions, the dashed field to the predicted amphibolite-facies assemblage for a fully equilibrated hydrated eclogite. Garnet and hornblende compositions are as analyzed in the domains described. Minerals preserved only as relics of HP stage are indicated in brackets. Since only quartz was removed from the initially calculated bulk-compositions, C" and D" plot in the same location as C' and D', respectively. A" would plot on the A–C axis, because Fe and Mg were excluded from A".

bulk composition A', A" no longer includes FeO and MgO, and excess H_2O. For A", zoisite, lawsonite or both will be stable under these conditions (Fig. 7a). The modal abundance of zoisite never exceeds 70%, whereas a substantial excess H_2O along the prograde path will lead to almost 89% lawsonite of the total volume (Table 3). An equilibrium phase-diagram for bulk A" confirms that at high temperature and intermediate pressure, lawsonite breaks down to plagioclase (98%), with traces of corundum and sillimanite (Fig. 7b, Table 3). Where Fe and Mg are taken into account, sillimanite would be replaced by Fe–Mg-bearing spinel (Fig. 6). Pure lawsonite would break down to pure anorthite and vapor, whereas pure zoisite breaks down to anorthite (68%), grossular (29%) and corundum (3%). In view of the shape of the domain and the close compositional match, a lawsonite porphyroblast is the most likely precursor for domain A. The formation of porphyroblasts of lawsonite under equilibrium conditions sets narrow P–T limits (Fig. 7b) for the prograde path of evolution of this type of domain. Note that the fluid liberated upon breakdown of lawsonite and zoisite is assumed to have escaped and thus was no longer available on the retrograde path.

Domain B: Kyanite and Staurolite

Characterization of the domain

Domain B has a core of kyanite intergrown with staurolite (Fig. 8, Table 1). The mantle is made up of plagioclase, ranging from An_{78} adjacent to kyanite, to An_{49} in contact with staurolite, to An_{26} at the outer rim (Figs. 8c, d). Around kyanite, a thin veneer of K-feldspar is locally present. The edge of the plagioclase mantle is defined by strings of low-Ca amphibole ($Cum_{64}Gru_{36}$), and outside is mostly quartz. Locally, a few grains of magnesiohornblende are present at the edge of the plagioclase mantle, which appears to be a product of alteration of cummingtonite. A few grains of ilmenite represent the only accessory phase in the domain. The problem of formulating a model composition

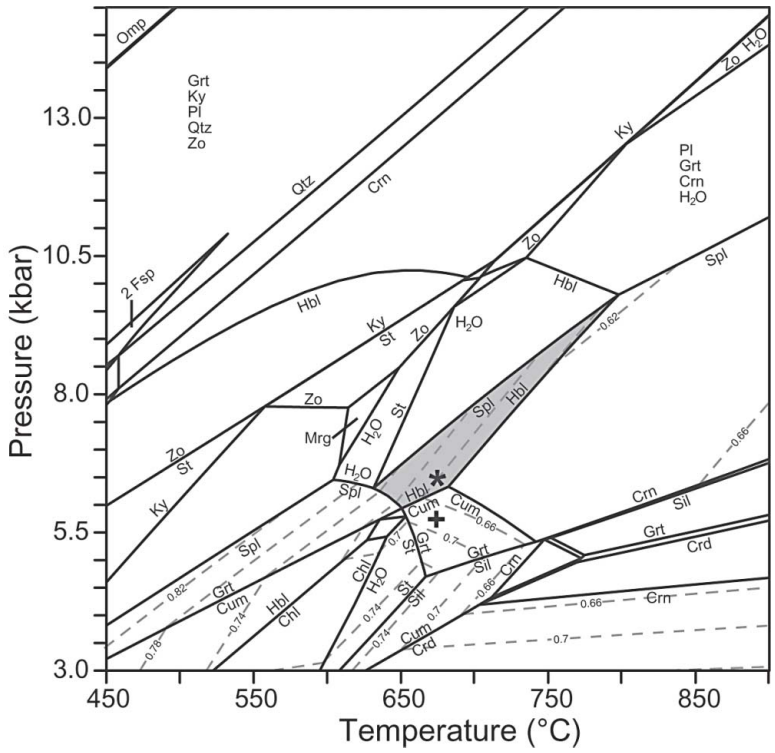

FIG. 6. CNFMASH equilibrium phase-diagram, domain A, bulk A'. For a few fields of stability, the stable assemblage of minerals is listed, in order of modal abundance. Star and plus symbols indicate conditions for which the predicted stable assemblage, including modal abundance and mineral compositions, is listed in Table 3. The symbols do not represent a P–T path for the rocks studied.

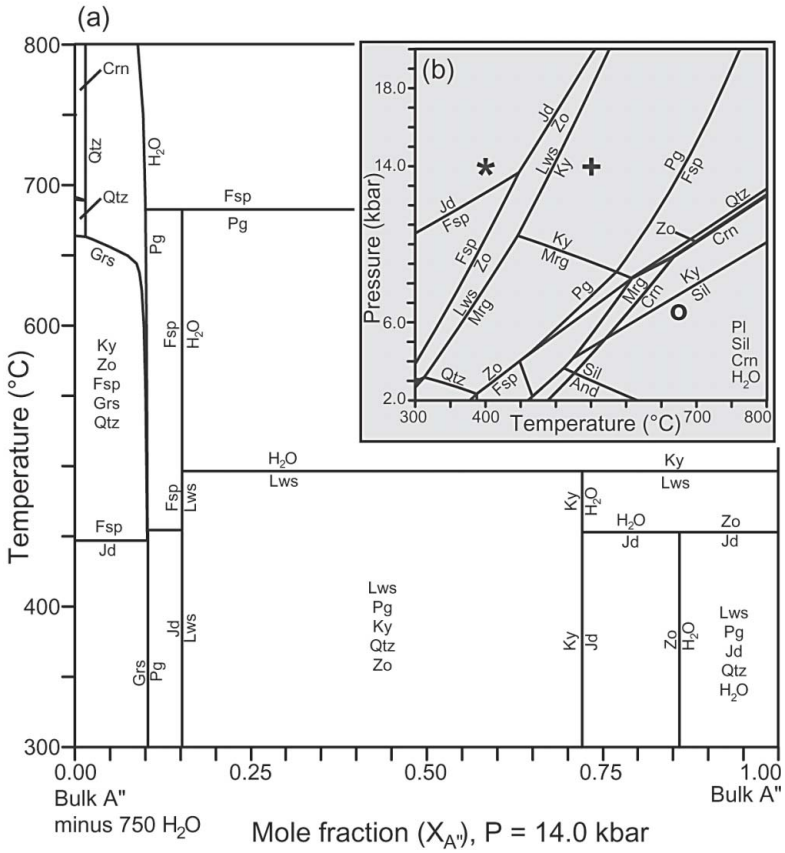

FIG. 7. (a) Binary diagram for H_2O *versus* T with bulk A" at 14 kbar, in CNASH. (b) Inset: CNASH equilibrium phase-diagram for bulk A" (wet), indicating the stability field of lawsonite and breakdown sequence to high temperatures. Star, circle and plus symbols refer to predicted stable assemblages listed in Table 3.

for this domain (as well as C and D) stems from the strong compositional zoning of the plagioclase shell. A composition of $X_{An} = 0.33$ was selected using compositional profiles (Figs. 8c, d), being representative of the spread of data and the thickness of each zone.

Model for the retrograde assemblage

The estimated bulk-composition of this domain (B' in Table 2, Fig. 5) yields an equilibrium phase-diagram in which the stability field of the observed assemblage of minerals is constrained by the absence of chlorite (>520°C), and the presence of staurolite (<670°C, Fig. 9). Isopleths for the composition of staurolite suggest that it formed between 540 and 630°C. The presence of kyanite and cummingtonite indicates pressures between 4 and 10 kbar. An additional constraint indicating a pressure below 9 kbar is imposed by the absence of hornblende and garnet from domain B. However, because the calculations only predict very small modal amounts of hornblende and garnet, that limit is less certain, especially since these phases might be present outside the plane of the thin section. The predicted modes and compositions closely correspond to those determined in domain B (Table 3). The formation of magnesiohornblende at the expense of cummingtonite is predicted to have occurred soon after cooling below the inferred conditions of equilibration (Fig. 9). We note, however, that no chlorite formed inside the domain, probably for lack of sufficient aqueous fluid.

Precursor

The equilibrium assemblage predicted by the program THERIAK for the bulk composition of domain B at 700°C and 20 kbar is dominated by 48 vol.% omphacite and 22% kyanite (Table 3). These conditions of high-pressure metamorphism were chosen to approximate previous estimates from the area (*e.g.*, Brouwer 2000, Tóth *et al.* 2000). If less SiO_2 is included in the domain, the abundance of free quartz is affected, with little influence on the relative abundances of the other phases. There is no single obvious precursor phase for this domain, but since kyanite porphyroblasts make up a fairly small part of the volume of kyanite eclogites, it is likely

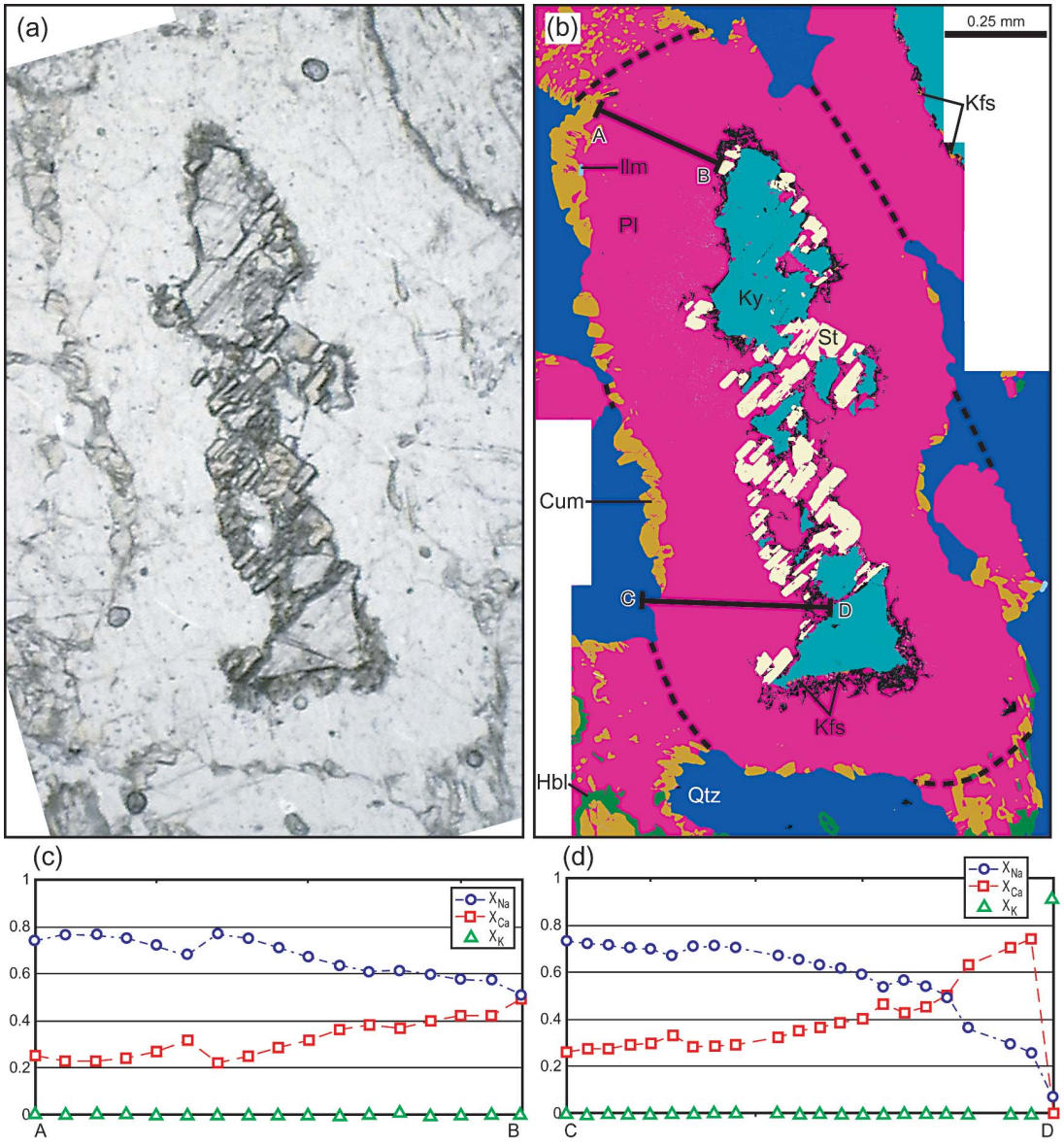

FIG. 8. Domain B. (a) Photograph of a thin section in plane-polarized light. (b) Back-scattered SEM image with indexed colors. (c, d) Variation of plagioclase components (electron-microprobe data) along the transects indicated in Figure 8b.

that this domain formed where a kyanite porphyroblast interacted with neighboring omphacite. Material-transfer analysis confirms the conclusion reached by Godard & Mabit (1998) that omphacite must be involved in the formation of corundum, Fe–Mg-bearing spinel and sapphirine-bearing symplectites after kyanite.

Domain C: Garnet and Corundum

Characterization of the domain

Domains C and D are neighbors in sample AA97–14.2 (Figs. 10a, b). In the core of domain C (lower left in Fig. 10b), a grain of garnet and many grains of corundum are distributed among phlogopite grains in a matrix of plagioclase ($An_{36–54}$). The garnet has a fairly flat zoning pattern, with $Alm_{52}Grs_{25}Prp_{21}Sps_2$ in a broad core zone, and a 30-μm rim with the composition grading to $Alm_{57}Grs_{19}Prp_{18}Sps_6$ at the edge. The mantle consists mostly of plagioclase, with inclusions of magnesiohornblende, orthopyroxene ($En_{58}Fs_{39}$) and quartz near the outer edges. Plagioclase in the mantle ranges from An_{55} at the rim of garnet to An_{16} on the outside (Fig. 10d). Again, the plagioclase mantle is rimmed by quartz. A few grains of rutile are included in garnet, whereas ilmenite is present in the rest of the domain. Locally, chlorite occurs as a retrograde replacement of phlogopite.

Model for the retrograde assemblage

The initial models for this domain indicated that only little quartz may be included in the reconstruction of the bulk composition of the domain, because otherwise up to 7 vol.% of kyanite or sillimanite would be predicted, whereas neither phase is present within the domain. In addition, small amounts of quartz produce a relatively large joint field of stability for garnet, corundum and biotite (Fig. 11, for quartz-free bulk C", Table 2). To

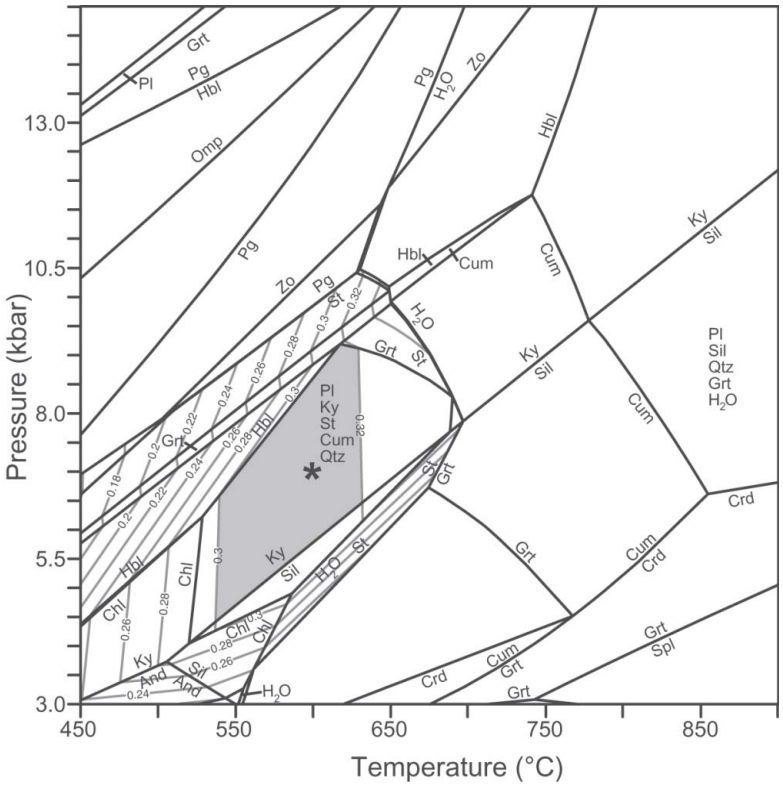

FIG. 9. Calculated CNFMASH equilibrium phase-diagram delimiting the stability fields of all mineral assemblages for domain B with bulk composition B' (Table 2). Isopleths for Mg in staurolite. The predicted stable assemblage of minerals in the shaded field is listed in order of modal abundance. Star symbol refers to predicted stable assemblage listed in Table 3.

reach an adequate match of prediction and observation, the bulk composition was adjusted slightly from the initial estimate (C' in Table 2, Fig. 5, with 6 vol.% quartz included).

Our preferred model for the current domain predicts equilibration temperatures above 700°C owing to the absence of staurolite (Fig. 11). The pressure is constrained between 5 and 11 kbar by the absence of white mica and Fe–Mg-bearing spinel from the domain (Figs. 10, 11). These constraints are considered firm, because in garnet, biotite and corundum, all three constraining phases have a likely precursor at whose expense they are likely to have formed. The presence of ilmenite instead of rutile in the domain matrix suggests equilibrium at 6.5 ± 1 kbar and T > 720°C. There is no upper temperature constraint in this domain, and higher temperatures would imply significantly higher pressures of equilibration. Higher temperatures, however, are considered unlikely in view of the relatively low temperatures of equilibration inferred for domain B, from a different sample collected from the same eclogite boudin.

The model fails to reproduce the observed composition of garnet in the stability field of biotite and corundum, but does so at significantly higher P and T (*e.g.*, at 700°C and 16 kbar, Table 3). The garnet in the domain is apparently the remaining core of a grain of garnet that was partly resorbed. We note that the composition of garnet and biotite cannot be used to determine exact P–T conditions of their formation, because exchange with hornblende, which affects garnet and biotite, cannot be modeled accurately. If calculated, the isopleth for the appropriate composition of biotite actually plots below the P–T field in Figure 11. The formation of orthopyroxene and magnesiohornblende in the rim of the domain is not easily explained with the current model. It is certainly possible that inadequacies of our amphibole solution-models are responsible for the failure to reproduce the observed phase-relations in detail. Alternatively, interaction with other domains outside the field of view or the plane sectioned could account for the minor discrepancy. In similar rocks, orthopyroxene has been reported where garnet abuts against a symplectite of sapphirine and plagioclase after kyanite (Carswell *et al.* 1989), or as a breakdown product of garnet or clinopyroxene or both (Johansson & Möller 1986).

Precursor

For the bulk composition of domain C at 700°C and 20 kbar, we computed with THERIAK a local equilibrium assemblage dominated by omphacite, white mica, and kyanite, with contributions of garnet, quartz and paragonite (Table 3). Again, a likely scenario is that a kyanite porphyroblast and its omphacite neighbors interacted to produce the present domain.

DOMAIN D: KYANITE AND HERCYNITE

Characterization of the domain

Domain D (top right in Fig. 10b) is dominated by a core of kyanite, surrounded by fine hercynite ($Hc_{75}Spl_{25}$) and coarser phlogopite (X_{Mg} in the range 0.59–0.66). These minerals are embedded in plagioclase, with a composition of $An_{52–63}$ between the kyanite grains, and ranging from An_{88} bordering kyanite to An_{17} at the outside edge (Fig. 10c). The most calcic plagioclase also has a small orthoclase component (2%). Beyond the plagioclase mantle, the domain is surrounded by quartz, with minor amounts of edenite and orthopyroxene ($En_{59}Fs_{38}$) occurring at the contact between plagioclase and quartz. Some grains of ilmenite are distributed among the hercynite strings.

Model for the retrograde assemblage

If some quartz is included in the estimated bulk-composition (D' in Table 2, Fig. 5), we compute with DOMINO an equilibrium phase-diagram in which the stability fields of Fe–Mg-bearing spinel and kyanite are separated by about 150°C and 4 kbar. Also, Fe–Mg-bearing spinel is predicted to be stable with cordierite, which is not observed in domain D, and at temperatures over 850°C, which seem exceedingly high. With no quartz in the domain (D" in Table 2), the stability fields are much closer, but still do not overlap (Fig. 12a).

One of the phlogopite samples in this domain has X_{Mg} equal to 0.64, and three others cluster around 0.60. If the former equilibrated with kyanite, this constrains the P–T conditions at 750 ± 25°C and 9.5 ± 1 kbar. Isopleths for hercynite in Fe–Mg-bearing spinel, and the disappearance of corundum define a stability field of hercynite at 720 ± 25°C and 5.0 ± 1 kbar, again inside the stability field of ilmenite. A binary phase-diagram for pressure *versus* SiO_2 contents indicates that the amount of quartz originally assumed to belong to this domain was slightly overestimated. Decompression from 8 to 5 kbar at about 700°C results in hercynite growth, while avoiding the corundum field (Fig. 12b), only if less than 3% (instead of the original 5%) of free quartz are included. We therefore interpret the formation of hercynite in domain D to result from the breakdown of garnet ± staurolite.

The model also predicts the growth of considerable amounts of sillimanite (Table 3), which is not observed in domain D. The transformation from kyanite to sillimanite may have been hindered by the limited availability of a fluid phase that could have enhanced the reaction kinetics. The biotite, with a phlogopite component around 0.60, as well as magnesiohornblende at the rim of the domain, likely have formed upon decompression (Fig. 12a). The observed presence of orthopyroxene

is not predicted by this model, which, as in domain C, may be due to the imperfection of our amphibole solution model or to minor chemical interaction with neighboring domains.

Precursor

For the quartz-free bulk composition (D") at 700°C and 20 kbar, we compute with THERIAK a local equilibrium assemblage made up mainly of omphacite (52%) and kyanite (30%) with some phengite and quartz, plus trace amounts of garnet, K-feldspar, titanite and rutile (Table 3). As in domain C, neighboring kyanite and omphacite porphyroblasts likely produced domain D upon partial hydration. The two neighboring grains of kyanite must have become separated during the early stages of symplectite development, after which they evolved as chemically distinct entities.

DISCUSSION

Metamorphic differentiation by prograde growth of porphyroblasts

The four types of domains documented and modeled above all represent compositionally distinct reaction volumes. If considered in the context of the matrix surrounding these domains, where the amphibolite assemblage forms a quite homogeneous fabric, the domains are unlikely to represent a porphyritic igneous texture. Instead, the present assemblages and modes of minerals inside each reaction domain, as well as their shapes, point to prograde growth of porphyroblasts as the most likely mechanism for domain formation. Lawsonite (and perhaps zoisite), kyanite, and garnet, are all likely to have appeared prior to the complete replacement of plagioclase by omphacite. The precise sequence of prograde reactions cannot be deciphered on the basis of the petrographic evidence alone, but comparison with phase diagrams computed for the pertinent bulk-compositions delimit both the prograde P–T path followed (Fig. 13a) and the reaction sequence likely experienced by sample Ma9338. If we assume an early hydration of the igneous basic protolith under (sub?)greenschist-facies conditions, lawsonite domains (Fig. 7b) then preceded the growth of garnet porphyroblasts (*e.g.*, Figs. 2, 11), and the domains of omphacite (Fig. 12) were established only after that. Overall, such small-scale metamorphic differentiation leads to a matrix (~60 vol.%) impoverished in Al_2O_3, CaO, and TiO_2 (Fig. 5).

Reactions during decompression

In the evolution following the eclogite-facies stage, the matrix assemblage must have been partially hydrated to hornblende, minor plagioclase and <5% quartz. The aqueous fluid gaining access to the relatively small boudins of eclogite (tens of meters in diameter) is likely to have been derived from crystallizing partial melts in the immediate vicinity, as migmatitic gneisses with up to 30 vol.% leucosome and occasional pegmatitic accumulations envelop the mafic lenses. Hydrous fluid expelled during crystallization of these granitic or tonalitic melts were certainly saturated in aqueous silica and possibly in feldspar components; hence some mass transfer into the basic boudins is probable. A sparse network of quartz veinlets is conspicuous in the Gorduno lens (Tóth *et al.* 2000), and assemblages documented from the immediate vicinity of these hydrofractured zones indicate a relatively high-pressure stage of interaction (*ca*. 700°C, 8–11 kbar). Yet it appears from the preservation of silica-poor assemblages in several of the domain types that the effect of this hydrothermal overprint was spatially very limited, possibly due to self-sealing by the positive $\Delta_r V_{solid}$ of the hornblende-forming reaction. The spatial separation of quartz-undersaturated domains from largely hydrated matrix containing free quartz is 20–30 μm wide, with calcic plagioclase making up most of the armor around the relics (Fig. 4). The equilibration volume calculated for decompression reactions at these conditions is smaller than 10^4–10^5 μm^3. Outside the domains, the homogeneity of the matrix, dominated by hornblende and plagioclase, indicates the presence of reaction volumes that are at least two or three orders of magnitude larger.

The chemical effectiveness of the differentiation established by porphyroblast growth and largely retained in the subsequent evolution of the domains is illustrated in Figure 5. The local chemical equilibration within previously fractionated chemical domains, with preservation of pseudomorphic precursors, such as lawsonite rhomboids in domain-type A, sets limits to the grain-scale mass transfer required for the irreversible reactions leading to inclusions of Al-rich phases such as corundum, kyanite, and staurolite. Whereas aluminum itself is relatively immobile, petrographic evidence in some cases points to indirect mechanisms for net reaction (Carmichael 1969) that assist in reducing local chemical disequilibrium. The topology of the domains investigated in this study (Figs. 4, 8, 10) might indicate that the most Al-rich product phases only survived in central parts of the domains and were replaced within the more or less concentric shells armoring the core. This inference requires more careful scrutiny. It may be correct for domain A, where the shell of intermediate plagioclase ($An_{30–40}$) is interpreted as a product of reaction derived from an originally larger porphyroblast of lawsonite and the surrounding matrix. For domain B, the petrographic evidence and reaction stoichiometries are compatible with a volume-by-volume mechanism of replacement of kyanite (plus eclogite matrix phases; Table 3) by staurolite (plus plagioclase and minor amphibole), if the overall net-transfer reaction (in CNFMASH) is written as being fluid-conservative:

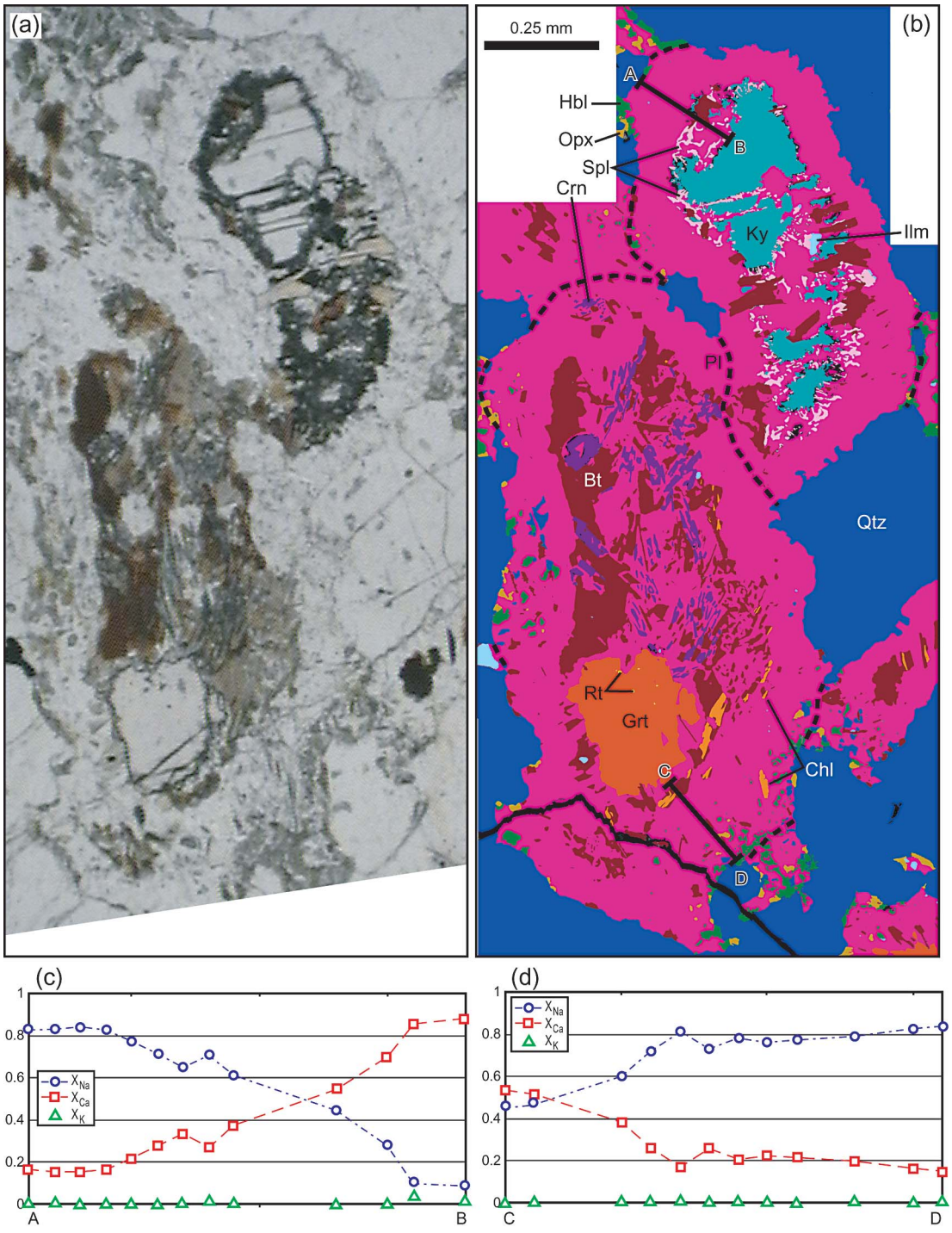

FIG. 10. Domains C (left in Figs. 9a and 9b) and D (right). (a) Photograph of a thin section in plane-polarized light. (b) Back-scattered SEM image with indexed colors. (c) Variation of plagioclase components (electron-microprobe data) in domain D, along the transect indicated in Figure 9b. (d) Variation of plagioclase components (electron-microprobe data) in domain C, along the transect indicated in Figure 10b.

89 Ky + 235 Cpx + 182 Qtz + 19 Zo + 3 Pg →
3 St + 276 Pl + 6 Amp (unit: moles)

Plagioclase is most Al-rich (*i.e.,* calcic) in the inner parts of the shell (An_{78} next to corroded kyanite, An_{49} next to newly formed staurolite), and the outermost part of the plagioclase rim (An_{26}) coexists with Al-free cummingtonite. Hence, whereas the overall replacement reaction is mass-balanced for composition B' (Table 3), the phase topology (Fig. 8) indicates a reaction mechanism that minimized the transport of Al away from the kyanite precursor. The outer part of the domain is *not* a rim of metasomatic plagioclase but a reaction product presumed to be in "closed system" equilibrium with the core of the domain. We note, however, that the zoning of the plagioclase indicates a chemical potential gradient between the outer rim and the core.

For domains C and D, more than one stage of net-transfer reaction is indicated (Fig. 10). In C, the quartz-undersaturated assemblage involving corundum may have formed early, from an eclogite assemblage saturated in quartz, in a first stage (20 → 16 kbar, Table 3) of a sequence of decompression reactions. Also, during that stage, garnet ($Alm_{52}Grs_{25}Prp_{21}Sps_2$) may have formed at the expense of kyanite and omphacite, whereas phlogopite (replacing phengite) and ilmenite replacing rutile (partially) were transformations of a second stage. The sequence by which these phases appear in the computed phase-diagram (Fig. 11) is in remarkably good agreement with the observed texture of the intergrowth in Figure 10, and again the plagioclase-rich shell of the domain can be considered to be part of the overall domain.

In D, finally, at least two stages of partial re-equilibration are preserved (Fig. 10). Tiny grains of hercynite outline what may have been the original boundary of a kyanite crystal, and ilmenite completely replaced rutile in the core part of the domain. The newly formed phases are not stable inside the kyanite field, yet sillimanite has not been observed. This absence is due either to slow kinetics of transformation of the Al-silicates or a two-stage reaction sequence, with hercynite growing from

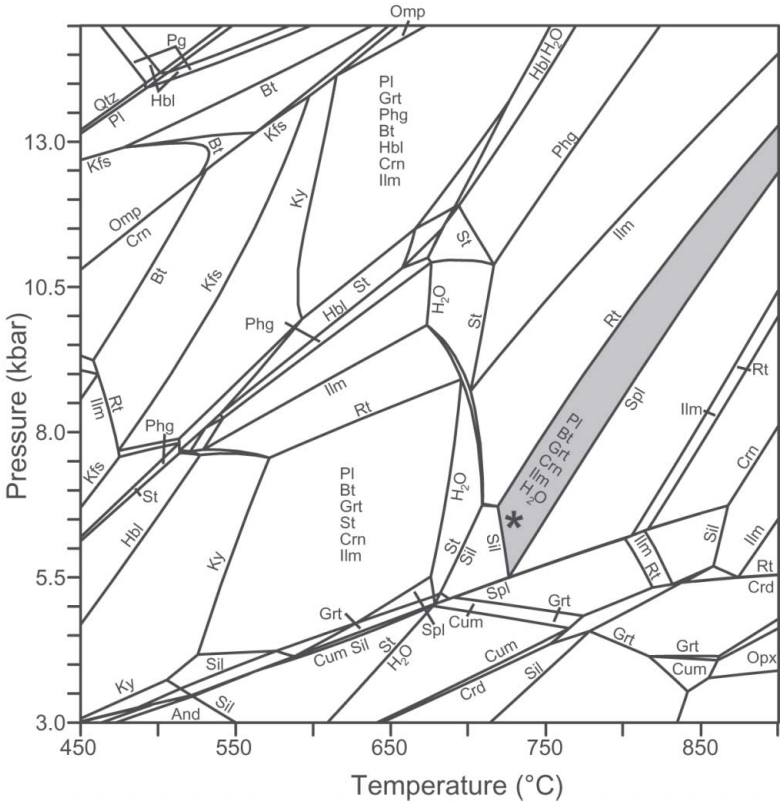

FIG. 11. Calculated TKCNFMASH equilibrium phase-diagram delimiting the stability fields of all mineral assemblages for domain C with bulk composition C" (Table 2). Star symbol refers to the predicted stable assemblage listed in Table 3.

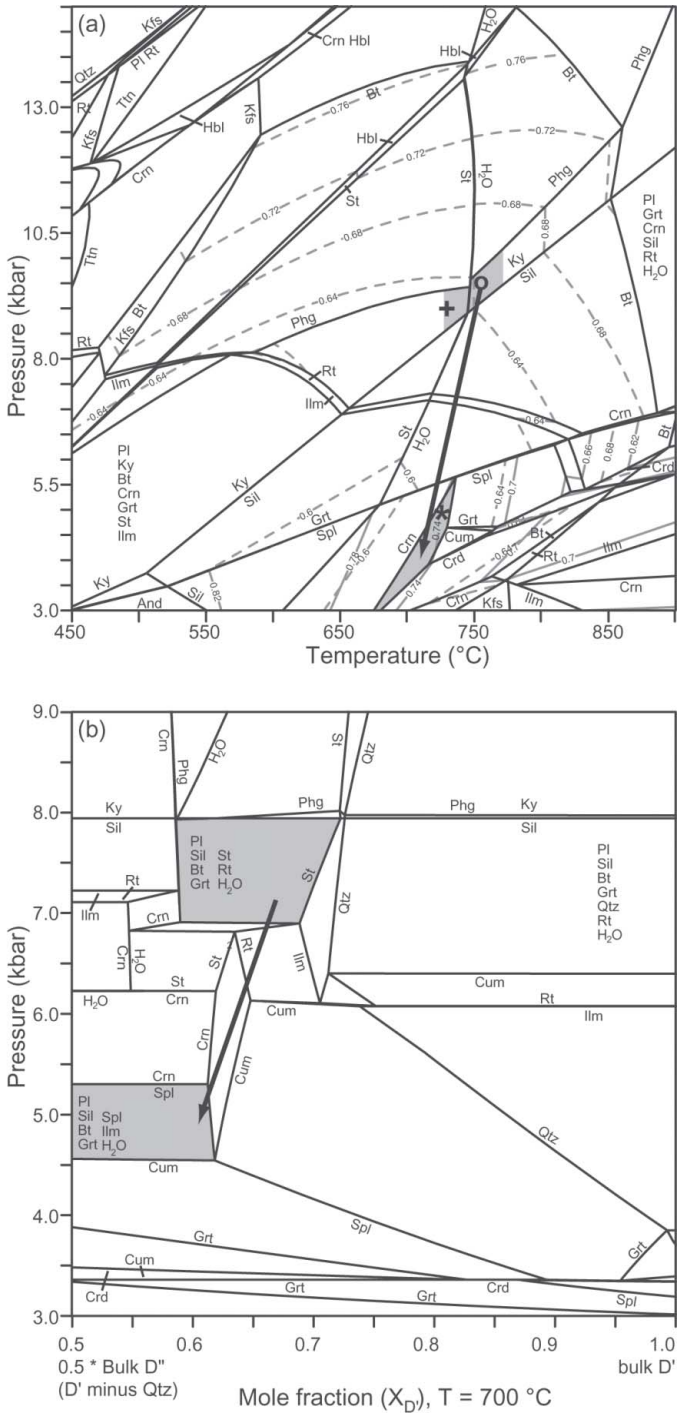

FIG. 12. (a) Calculated TKCNFMASH equilibrium phase-diagram delimiting the stability fields of all mineral assemblages for domain D with bulk composition D" (Table 2). Isopleths for phlogopite in biotite and hercynite in spinel. Star, circle and plus symbols refer to predicted stable assemblages listed in Table 3. (b) Binary join between 0.5 × bulk D" and bulk D', to show the role of quartz.

corundum or staurolite. As in the previous examples (A, B), the plagioclase mantle around the Al-rich core portion is strongly zoned. In this case, the inner portion spans the range from almost pure anorthite (An_{88}) to An_{55}, the outer portion starts at An_{38} and is continuously zoned to An_{18}. This outer part thus shows zoning that starts at the Bøggild gap and ends at the peristerite gap in the phase diagram for albite–anorthite. Overall, we interpret the distribution and compositional zoning of phases in domain D to be the result of net-transfer reactions in which Al-transport was minimized. The plagioclase armor surrounding the partially re-equilibrated central portion shows zoning which we attribute to local equilibration in a chemical gradient.

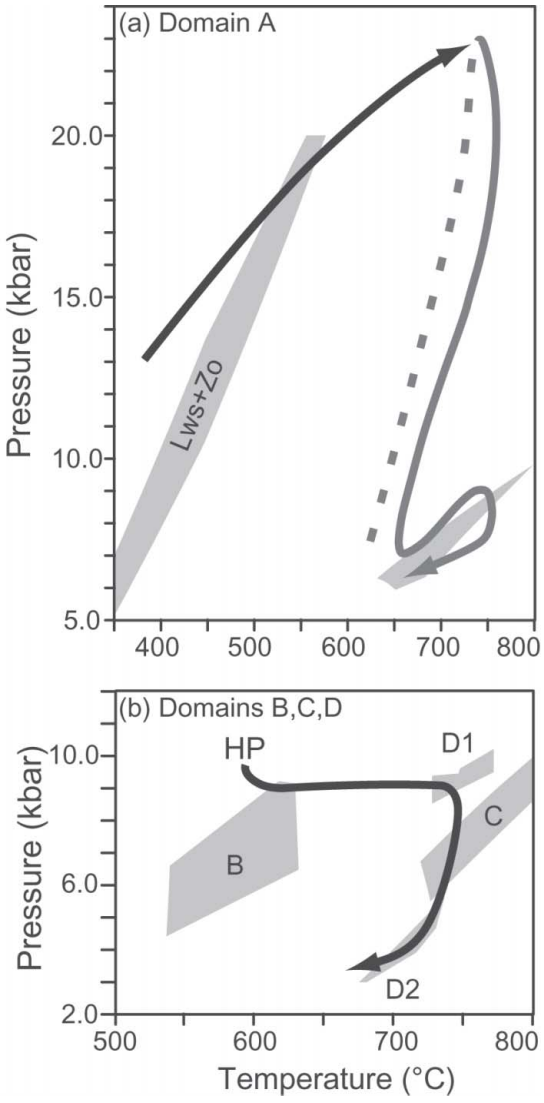

FIG. 13. (a) Estimates of P–T evolution, domain A; P–T trajectory in grey from Tóth *et al.* (2000) for this same lens. The prograde path is now constrained to blueschist-facies conditions, owing to evidence of a lawsonite precursor in domain A. (b) P–T estimates for the partial equilibration of domains B, C and D, from another boudin of eclogite in the same mélange zone. Note the different scales of temperature in a and b.

In previous studies, several investigators have put forward hypotheses to explain the presence of minerals like Fe–Mg-bearing spinel, corundum, and sapphirine in kyanite eclogites. Observations of granulite-facies reaction zones 50–100 μm across along veins in Norwegian eclogites suggest localized fluid-assisted re-equilibration along hydrofractures, leaving the remainder of the eclogite body unchanged (Straume & Austrheim 1999). However, because in our samples hornblende is a dominant phase outside the domains, and the reaction volumes are substantially larger, this model does not explain the textures observed. In other cases, extensive progress of reactions for quartz-undersaturated bulk compositions under granulite-facies conditions led to the formation of sapphirine–plagioclase symplectites after kyanite, but also after garnet and clinopyroxene (Carswell *et al.* 1989, Godard & Mabit 1998). The observation that domains B, C, and D are surrounded by quartz disqualifies this model for the present case. In addition to the internal texture of the domains studied, the presence of quartz and calcic amphibole in the surrounding matrix renders our symplectites very similar to those described in a kinetic model for the formation of plagioclase coronas around kyanite (Nakamura 2002). In the present study, our thermodynamic modeling with DOMINO and THERIAK, using the estimated bulk compositions of four quite different symplectite domains, proves to be successful in reproducing the observed assemblages of minerals. Therefore, the assumptions of local equilibrium and restricted volume of equilibration during symplectite formation, on which the Nakamura model is based in part, are warranted.

Decompression paths inferred for lenses inside the tectonic accretion channel

The models presented above for four domains in kyanite eclogites from the Central Alps yield new constraints on the P–T trajectories of the boudins from which they were collected. The mineral assemblage in domain A (Loc. 1, Fig. 1b) yields conditions of equilibration of 675 ± 25°C and 6.5 ± 1 kbar. This sample was also included in the analysis of Tóth *et al.* (2000), and the present results provide additional constraints on the P–T trajectory derived in that paper (Fig. 13). The rocks were shown to have undergone high-pressure metamorphism at 23 ± 3 kbar and 750 ± 50°C, subsequently cooled during rapid decompression to 675 ± 25°C at 8 ± 1 kbar, before a final heating phase at simi-

lar pressures and 750 ± 40°C. The present result suggests that initial cooling proceeded to somewhat lower pressures. Importantly, our analysis indicates that lawsonite is the most likely precursor for the domain, implying that the subduction took place in a much cooler setting than previously considered (Fig. 4b).

Domains B, C and D stem from a single boudin (Loc. 2, Fig. 1b), and although they have recorded somewhat different conditions of equilibration, they share the same P–T trajectory. The estimated conditions of equilibration for the three domains constrain the Barrovian metamorphic stage, as experienced by these samples (Fig. 13). The arrow indicates a trajectory that the boudin is likely to have followed, although the temperature recorded by domain C may actually have been up to 100°C higher. High-pressure metamorphism and initial decompression thus were followed by a stage of near-isobaric heating to about 750°C, which has also been reported previously from other bodies of eclogite in the area (*e.g.,* Brouwer 2000, Tóth *et al.* 2000). An investigation of other domain types from this eclogite lens may yield further constraints on the P–T conditions during subduction, high-pressure metamorphism and initial decompression in the mélange sequence from which the samples were taken. Owing to its different chemical composition, these conditions did not lead to the stabilization of hercynite-dominant spinel or corundum in domain B (Fig. 8). In any case, the P–T conditions for the Barrovian overprint recorded in this lens are above 700°C between about 9 and 4 kbar. This temperature is only slightly higher than that recorded in the same area for the regional Tertiary overprint, for pressure conditions of 5.5–6 kbar (Todd & Engi 1997).

Uncertainties in the approach

A major uncertainty involved in thermodynamic modeling of mineral assemblages is related to the thermodynamic database used. The current weakness of solution models to adequately describe complex amphiboles, and the limited applicability of solution models for clinopyroxene at temperatures below about 500°C limit the types of assemblages that can be modeled. In the four domains presented here, amphibole is present in very small amounts only (<2 vol.%). The pargasite – actinolite solution model adopted here yields only an approximate description of the magnesiohornblende present, but owing to the low modal abundance, this inaccuracy should not affect the other phases very strongly. We note, however, that isopleths for the composition of amphiboles cannot be used to infer exact conditions of equilibration.

A second uncertainty lies in the determination of the "bulk" compositions of domains. The models presented above closely approximate the observed assemblages of minerals, which suggests that determining the domain boundaries optically, and iterative adjustment based on model results, have been effective. Analysis of back-scattered electron images yields accurate estimates of the surface area of each phase present. The assumption that surface area in thin sections can be directly converted to modal volume is apparently valid for the kind of texture studied. The choice of an average composition for each phase which, when combined with their modal volume, yields an estimate for the chemical composition of the domains, introduces additional uncertainty. Electron-microprobe data for the individual phases, an assessment of the variety of each mineral, and zoning patterns support an appropriate choice, which is in some cases hampered by the small size of grains in the symplectites. Finally, the amount and composition of fluids present at the time of mineral reaction (or re-equilibration) are difficult to assess, although in some cases, an identified precursor phase, such as lawsonite in domain A, imposes limits (Fig. 7a). In other cases, a variety of preliminary scenarios may be formulated, depending on the availability of fluids, which possibilities can then be assessed by calculating binary phase-diagrams, with variable amounts of the volatile component present, as a function of pressure or temperature.

Conclusions

Kyanite eclogites develop plagioclase symplectites involving high-Al phases like corundum, Fe–Mg-bearing spinel and, in rare cases, staurolite, which would not normally be expected in rocks of mafic bulk-composition. Thermodynamic modeling of such domains in eclogites from the Central Alps indicates that during decompression, such phases can develop where the equilibration volume involving porphyroblasts is restricted, rendering the effective bulk-composition distinctly different from that of a normal MORB-type basalt. Accurate estimates of domain composition are obtained by combining image analysis with electron-microprobe data, and may be refined in an iterative process during which mineral assemblages predicted by thermodynamic models are compared with observations. The fact that even models based on initial estimates of domain composition reproduce most features of the domains studied supports this approach, and indicates that the basic assumption of local equilibrium is probably tenable. Once the domains are accurately documented, thermodynamic models are used to analyze the conditions at which the symplectites developed, and in some cases precursor phases can be inferred. In three samples analyzed in detail, lawsonite and kyanite porphyroblasts formed at the prograde stage. Local textures produced on the decompression path and quantitative phase-relations for that stage indicate small reaction-volumes and minimum distances of transport of Al-carrier species.

The results of this analysis, applied to kyanite eclogite samples from the Southern Steep Belt of the Central Swiss Alps, provides new constraints on pro-

grade and retrograde P–T paths, and they confirm late-stage heating at mid-crust depths.

Acknowledgements

It is our pleasure to acknowledge particularly perceptive comments on this manuscript from Dugald M. Carmichael, to whom we dedicate this paper. He has guided us and a generation of petrologists by his studies, combining astute observation, eloquent descriptions, and rigorous thinking, and we have all been blessed with his joyful personality.

Discussions with Alfons Berger and Tom Burri, and analytical assistance from Nicola Bistacchi have contributed to the substance of this study. Thoughtful reviews by Marc R. St-Onge and Encarnación Puga, as well as careful editorial comments from Robert F. Martin, have helped us improve the presentation. Financial support from Schweizerischer Nationalfonds (No. 20–63593.00 and 20020–101826) is gratefully acknowledged.

References

Bächlin, R., Bianconi, F., Codoni, A., Dal Vesco, E., Knoblauch, P., Kündig, E., Reinhard, M., Spaenhauer, F., Spicher, A., Trommsdorff, V. & Wenk, E. (1974): Geologischer Atlas der Schweiz, 1:25 000, Blatt 1313 Bellinzona. Schweizerische Geologische Kommission, Bern, Switzerland.

Berman, R.G. (1988): Internally-consistent thermodynamic data for minerals in the system Na_2O–K_2O–CaO–MgO–FeO–Fe_2O_3–Al_2O_3–SiO_2–TiO_2–H_2O–CO_2. *J. Petrol.* **29**, 445-522.

Bocchio, R., Liborio, G. & Mottana, A. (1985): Petrology of the amphibolitized eclogites of Gorduno, Lepontine Alps, Switzerland. *Chem. Geol.* **50**, 65-86.

Brouwer, F.M. (2000): *Thermal Evolution of High-Pressure Metamorphic Rocks in the Alps*. Ph.D. thesis, Utrecht University. *Geologica Ultraiectina* **199**, 221 p.

Carmichael, D.M. (1969): On the mechanism of prograde metamorphic reactions in quartz-bearing pelitic rocks. *Contrib. Mineral. Petrol.* **20**, 244-267.

Carpenter, M.A. (1985): Order–disorder transformations in mineral solid solutions. *In* Microscopic to Macroscopic: Atomic Environments to Mineral Thermodynamics (S.W. Kiefer & A. Navrotsky, eds.). *Rev. Mineral.* **14**, 187-223.

Carswell, D.A., Möller, C. & O'Brien, P.J. (1989): Origin of sapphirine–plagioclase symplectites in metabasites from Mitterbachgraben, Dunkelsteinerwald granulite complex, Lower Austria. *Eur. J. Mineral.* **1**, 455-466.

Dal Vesco, E. (1953): Genesi e metamorfosi delle rocce basiche e ultrabasiche nell'ambiente mesozonale dell'orogene pennidico: studio geologico-petrografico della catena Gaggio-Basal (cantone Ticino). *Schweiz. Mineral. Petrogr. Mitt.* **33**, 173-480.

De Capitani, C. (1994): Gleichgewichts-Phasendiagramme: theorie und Software. *Eur. J. Mineral.* **6** Beiheft, 48 [http://titan.minpet.unibas.ch/minpet/groups/theriak/theruser.html].

Elvevold, S. & Gilotti, J.A. (2000): Pressure–temperature evolution of retrogressed kyanite eclogites, Weinschenk Island, North-East Greenland Caledonides. *Lithos* **53**, 127-147.

Enami, M. & Zang, Q. (1988): Magnesian staurolite in garnet–corundum rocks and eclogite from the Donghai district, Jiangsu province, east China. *Am. Mineral.* **73**, 48-56.

Engi, M. (1983): Equilibria involving Al–Cr spinel. I. Mg–Fe exchange with olivine; experiments, thermodynamic analysis, and consequences for geothermometry. *Am. J. Sci.* **283-A**, 29-71.

_____, Berger, A. & Roselle, G.T. (2001): Role of the tectonic accretion channel in collisional orogeny. *Geology* **29**, 1143-1146.

Ghiorso, M.S., Evans, B.W., Hirschmann, M.M. & Yang, Hexiong (1995): Thermodynamics of the amphiboles; Fe–Mg cummingtonite solid solution. *Am Mineral.* **80**, 502-519.

Godard, G. & Mabit, J.-L. (1998): Peraluminous sapphirine formed during retrogression of a kyanite-bearing eclogite from Pays de Léon, Armorican Massif, France. *Lithos* **43**, 15-29.

Grubenmann, U. (1908): Granatolivinfels des Gordunotales und seine Begeleitgesteine. *Viertelj. Naturf. Ges. Zürich* **53**, 129-156.

Heinrich, C.A. (1986): Eclogite facies regional metamorphism of hydrous mafic rocks in the Central Alpine Adula nappe. *J. Petrol.* **27**, 123-154.

Johansson, L. & Möller, C. (1986): Formation of sapphirine during retrogression of a basic high-pressure granulite, Western Gneiss region, Norway. *Contrib. Mineral. Petrol.* **94**, 29-41.

Kretz, R. (1983): Symbols for rock-forming minerals. *Am. Mineral.* **68**, 277-279.

Lappin, M.A. (1960): On the occurrence of kyanite in the eclogites of the Selje and Åheim districts, Nordfjord. *Nor. Geol. Tidsskr.* **40**, 289-296.

Liati, A. & Seidel, E. (1994): Sapphirine and högbomite in overprinted kyanite-eclogites of central, N. Greece: first evidence of granulite-facies metamorphism. *Eur. J. Mineral.* **6**, 733-738.

Mäder, U.K. & Berman, R.G. (1992): Amphibole thermobarometry: a thermodynamic approach. *Geol. Surv. Can., Pap.* **92–1E**, 393-400.

MEYRE, C., DE CAPITANI, C. & PARTZSCH, J.H. (1997): A ternary solid solution model for omphacite and its application to geothermobarometry of eclogites from the Middle Adula nappe (Central Alps, Switzerland). *J. Metamorph. Geol.* **15**, 687-700.

_____, _____, ZACK, T. & FREY, M. (1999): Petrology of high-pressure metapelites from the Adula nappe (Central Alps, Switzerland). *J. Petrol.* **40**, 199-213.

MÖCKEL, J.R. (1969): Structural petrology of the garnet-peridotite of Alpe Arami (Ticino, Switzerland). *Leidse Geol. Meded.* **42**, 61-130.

NAGEL, T. (2002): *Metamorphic and Structural History of the Southern Adula Nappe* (*Graubünden, Switzerland*). Ph.D thesis, Geologisch-Paläontologischen Institut, University of Basel, Basel, Switzerland.

NAKAMURA, D. (2002): Kinetics of decompressional reactions in eclogitic rocks – formation of plagioclase coronas around kyanite. *J. Metamorph. Geol.* **20**, 325-333.

PFIFFNER, M. & TROMMSDROFF, V. (1998): The high-pressure ultramafic-mafic-carbonate suite of Cima Lunga–Adula, Central Alps: excursions to Cima di Gagnone and Alpe Arami. *Schweiz. Mineral. Petrog. Mitt.* **78**, 337-354.

SABAU, G., ALBERICO, A. & NEGELESCU, E. (2002): Peraluminous sapphirine in retrogressed kyanite-bearing eclogites from the South Carpathians: status and implications. *Int. Geol. Rev.* **44**, 859-876.

SCHMID, S.M., AEBLI, H.R., HELLER, F. & ZINGG, A. (1989): The role of the Periadriatic Line in the tectonic evolution of the Alps. *In* Alpine Tectonics (M.P. Crawford, D. Dietrich & R.G. Park, eds.). *Geol. Soc., Spec. Publ*. **45**, 153-171.

_____, PFIFFNER, O.A., FROITZHEIM, N., SCHÖNBORN, G. & KISSLING, E. (1996): Geophysical-geological transect and tectonic evolution of the Swiss–Italian Alps. *Tectonics* **15**, 1036-1064.

STRAUME, Å.K. & AUSTRHEIM, H. (1999): Importance of fracturing during retro-metamorphism of eclogites. *J. Metamorph. Geol.* **17**, 637-652.

TODD, C.S. & ENGI, M. (1997): Metamorphic field gradients in the Central Alps. *J. Metamorph. Geol.* **15**, 513-530.

TÓTH, T.M., GRANDJEAN, V. & ENGI, M. (2000): Polyphase evolution and reaction sequence of compositional domains in metabasalt: a model based on local chemical equilibrium and metamorphic differentiation. *Geol. J.* **35**, 163-183.

Received October 22, 2003, revised manuscript accepted June 22, 2004.

APPENDIX 1. ABBREVIATIONS USED FOR MINERALS AND END MEMBERS IN FIGURES AND TABLES

Ab	albite
Alm	almandine
And	andalusite
Apt	apatite
Bt	biotite series (phlogopite – annite solid solution)
Cel	celadonite
Chl	chlorite (clinochlore – chamosite solid solution)
Crd	cordierite (including sekaninaite, the Fe-dominant analogue)
Crn	corundum
Cum	cummingtonite – grunerite amphibole
Di	diopside
FeCel	ferroceladonite
Fsp	albite – anorthite – orthoclase feldspar
Grs	grossular
Grt	almandine – grossular – pyrope garnet
H_2O	water or steam
Hbl	hornblende, including actinolite and pargasite
Hc	hercynite
Hd	hedenbergite
Ilm	ilmenite
Jd	jadeite
K-phase	unidentified potassium-dominant phase
Kfs	albite – orthoclase feldspar
Ky	kyanite
Lws	lawsonite
Mrg	margarite
Ms	muscovite
Ol	olivine (fayalite – forsterite solid solution)
Omp	omphacite (jadeite – diopside – hedenbergite solid solution; clinopyroxene)
Opx	orthopyroxene (enstatite – ferrosilite solid solution)
Pg	paragonite
Phg	muscovite – celadonite – ferroceladonite solid solution (white mica)
Pl	plagioclase (albite – anorthite solid solution)
Prp	pyrope
Qtz	quartz
Rt	rutile
Sil	sillimanite
Spl	spinel (*sensu lato*; spinel – hercynite solid solution)
St	staurolite (including the Mg-dominant compositions, magnesiostaurolite)
Ttn	titanite
Zo	zoisite

APPENDIX 2. AVERAGE COMPOSITION OF THE MINERALS PRESENT IN EACH DOMAIN (NORMALIZED TO 100%), USED AS BASIS FOR ESTIMATE OF DOMAIN COMPOSITION

Domain A	Pl An_{90}	Crn	Hbl X_{Mg} 0.68	Ilm	K-phase +Pl mixed	Ms	Spl Hc_{70}
SiO_2 wt%	44.87		48.06	0.01	53.39	45.20	
TiO_2	0.01		0.66	50.28	0.00	0.01	
Al_2O_3	35.65	100.00	8.66	0.00	28.74	37.54	61.92
Cr_2O_3	0.01		0.07	0.07	0.01	0.01	
Fe_2O_3	0.12		0.72	4.58	0.03	1.07	
FeO	0.00		11.98	43.58	0.01	0.00	30.89
MnO	0.01		0.23	1.31	0.00	0.01	
MgO	0.02		14.04	0.07	0.01	0.33	7.10
CaO	18.14		12.03	0.09	10.64	0.07	
Na_2O	1.14		1.12	0.02	1.64	0.26	
K_2O	0.04		0.37	0.01	5.53	10.97	
H_2O			2.07			4.54	
Total	100.00	100.00	100.00	100.00	100.00	100.00	100.00

Domain B	Pl An_{33}	Cum X_{Mg} 0.64	Hbl X_{Mg} 0.61	Ilm	Kfs Or_{92}	Ky	Qtz	St X_{Mg} 0.31
SiO_2 wt%	59.79	55.07	46.57	0.02	63.48	36.76	100.00	27.14
TiO_2	0.01	0.09	0.90	44.92	0.00	0.01		0.31
Al_2O_3	25.27	1.48	10.28	0.00	20.59	62.63		55.15
Cr_2O_3	0.01	0.03	0.02	0.12	0.00	0.01		0.01
Fe_2O_3	0.22	0.00	0.07	14.71	0.00	0.54		
FeO	0.02	19.92	15.69	39.71	0.12	0.00		11.95
MnO	0.02	0.50	0.26	0.40	0.00	0.02		0.15
MgO	0.05	20.09	13.80	0.04	0.01	0.02		3.06
CaO	6.84	0.60	8.75	0.03	0.19	0.01		0.03
Na_2O	7.69	0.13	1.39	0.03	0.72	0.01		0.02
K_2O	0.07	0.00	0.23	0.01	14.88	0.00		0.01
H_2O		2.09	2.05					2.18
Total	100.00	100.00	100.00	100.00	100.00	100.00	100.00	100.00

Domain C	Pl An_{31}	Bt X_{Mg} 0.59	Chl+Bt mix X_{Mg} 0.60	Crn	Grt Grs_{23} Alm_{53} Prp_{22}	Hbl X_{Mg} 0.67	Ilm	Opx X_{Mg} 0.60	Qtz	Rt
SiO_2 wt%	60.22	35.70	32.32	0.01	38.46	47.80	0.05	52.88	99.81	
TiO_2	0.10	2.71	0.90	0.02	0.06	1.76	51.16	0.04	0.00	100.00
Al_2O_3	24.98	18.72	21.23	99.10	22.09	8.07	0.00	0.50	0.01	
Cr_2O_3	0.01	0.00	0.01	0.00	0.01	0.03	0.01	0.03	0.02	
Fe_2O_3	0.07	0.00	21.95	0.82	0.23	0.00	3.36	0.00	0.13	
FeO	0.21	15.89	0.00	0.00	24.09	12.80	43.92	24.66	0.00	
MnO	0.01	0.10	0.13	0.00	1.05	0.18	1.33	0.71	0.00	
MgO	0.15	12.72	16.29	0.00	5.55	14.29	0.05	20.84	0.00	
CaO	6.34	0.04	0.12	0.01	8.43	11.00	0.03	0.31	0.01	
Na_2O	7.72	0.13	0.03	0.00	0.02	1.35	0.01	0.02	0.01	
K_2O	0.18	10.02	2.78	0.02						
H_2O		3.95	4.23			2.05				
Total	100.00	100.00	100.00	100.00	100.00	100.00	100.00	100.00	100.00	100.00

Domain D	Pl An_{32}	Bt X_{Mg} 0.32	Hbl X_{Mg} 0.64	Ilm	Ky	Opx X_{Mg} 0.60	Qtz	Spl Hc_{75}
SiO_2	60.04	35.40	46.79	0.02	36.65	52.88	99.84	0.43
TiO_2	0.02	3.13	0.66	51.28	0.01	0.04	0.01	0.03
Al_2O_3	25.39	19.58	9.14	0.00	62.59	0.50	0.01	59.71
Cr_2O_3	0.01	0.01	0.00	0.03	0.02	0.03	0.03	0.03
Fe_2O_3	0.03	0.00	0.00	2.93	0.69	0.00	0.09	0.84
FeO	0.10	14.78	13.85	44.09	0.00	24.66	0.00	32.82
MnO	0.01	0.09	0.20	1.10	0.02	0.71	0.00	0.43
MgO	0.01	12.87	14.02	0.44	0.01	20.84	0.00	5.55
CaO	6.58	0.03	10.92	0.10	0.02	0.31	0.01	0.10
Na_2O	7.66	0.13	1.67	0.00	0.01	0.02	0.01	0.02
K_2O	0.16	10.03	0.70	0.01	0.01	0.01	0.00	0.05
H_2O		3.96	2.04				0.00	
Total	100.00	100.00	100.00	100.00	100.00	100.00	100.00	100.00